

1 **Enhanced Sulfate Formation in Mixed Biomass Burning and Sea-salt**
2 **Interactions Mediated by Photosensitization: Effects of Chloride,**
3 **Nitrogen-containing Compounds and Atmospheric Aging**

4 Rongzhi Tang^{1,2}, Jialiang Ma³, Ruifeng Zhang⁴, Weizhen Cui¹, Yuanyuan Qin⁵, Yangxi Chu⁶,
5 Yiming Qin¹, Alexander L. Vogel³, Chak K. Chan^{4,*}

6 ¹ School of Energy and Environment, City University of Hong Kong, Hong Kong, China

7 ² Shenzhen Research Institute, City University of Hong Kong, Shenzhen 518057, China

8 ³ Institute for Atmospheric and Environmental Sciences, Goethe-University Frankfurt, 60438
9 Frankfurt am Main, Germany

10 ⁴ Division of Physical Science and Engineering, King Abdullah University of Science and
11 Technology (KAUST), Thuwal 23955-6900, Kingdom of Saudi Arabia

12 ⁵ College of Resources and Environment, University of Chinese Academy of Sciences, Beijing,
13 100049, China

14 ⁶ State Key Laboratory of Environmental Criteria and Risk Assessment, Chinese Research
15 Academy of Environmental Sciences, Beijing, 100012, China

16 *Correspondence to:* Chak K. Chan (chak.chan@kaust.edu.sa)

17 **Abstract**

18 Discrepancies persist between modeled simulations and measured sulfate concentrations in
19 marine boundary layer, especially when the marine air was influenced by biomass burning
20 plumes. However, there is a notable dearth of research conducted on the interactions between
21 sea-salt aerosol and biomass burning plumes, impeding a comprehensive understanding of the
22 sulfate formation. This work studied sulfate formation by mixing real biomass burning (BB)
23 extracts and NaCl, mimicking internal mixtures of BB and sea-salt particles. Significant
24 enhancement of sulfate formation was observed for BB-NaCl particles compared to incense
25 burning (IS)-NaCl particles. For fresh particles, the sulfate formation rate followed the trend of
26 corn straw (CS)-NaCl>rice straw (RS)-NaCl>wheat straw (WS)-NaCl>IS-NaCl. The filter
27 aging was achieved by exposing them to OH• through UV irradiation. Aged particles showed
28 changes in sulfate formation rates, with the highest enhancement by RS-NaCl due to
29 interactions between RS and NaCl. Model experiments spiked with nitrogen-containing organic
30 compounds (NOCs), such as pyrazine (CHN) and 4-nitrocatechol (CHON), revealed positive
31 effects of chloride in the PS-CHON system and negative effects in the PS-CHN system. Our
32 work suggests that BB reaching or near coastal areas could affect sulfate formation via
33 photosensitizer-mediated reactions, potentially exacerbating air quality concerns.

34 **Keywords:** sulfate formation, biomass burning, photosensitization, sea-salt aerosol, chloride

35 1 Introduction

36 Recent fire outbreaks in areas like Canada, Amazonia, and Southeast Australia, together with
37 the increased fire frequency and intensity reports in areas like western US have highlighted the
38 risks of fire, especially biomass burning (BB), to human health and climate change (Bond et
39 al., 2013; Andreae, 2019; Jones et al., 2022). As an agricultural powerhouse, China boasts
40 immense agricultural crop yields, especially in rice, wheat, and corn throughout the country.
41 These crop residues are frequently burned in rural areas for cooking and heating purposes, as
42 well as for land preparation after harvest, resulting in the substantial production of light-
43 absorbing species, such as brown carbon (BrC) (Chen et al., 2017). Recent studies have reported
44 that specific BrC species from biomass burning, including vanillin (VL), acetovanillone,
45 syringaldehyde (SyrAld), and naphthalene-derived secondary organic aerosol (Teich et al.,
46 2016; Li et al., 2024; Liu et al., 2020; Wang et al., 2021b) can act as photosensitizers (PS) and
47 oxidize SO₂ to sulfate (Zhou et al., 2023; Liang et al., 2024). Atmospheric processes like aging
48 or long-range transport, can alter the chemical compositions and optical properties of PS, and
49 hence affect the sulfate formation potential (You et al., 2020; Li et al., 2019). Sea-salt aerosol
50 (SSA), with its high particulate matter loadings and extensive surface area, plays a significant
51 role in interfacial and multiphase reactions with reactive gases, thereby impacting global
52 radiation balance and air quality in marine and coastal areas (Gantt and Meskhidze, 2013; Chi
53 et al., 2015). Prior research has identified several secondary sulfate formation pathways in SSA,
54 e.g., multiphase SO₂ oxidation by O₃ (Alexander et al., 2012), coexistence of NO₂ (Zhang and
55 Chan, 2023b), PS (Tang et al., 2023), chlorine-PS synergistic effects (Zhang and Chan, 2024),
56 and Cl and OH radicals generated by chlorine photoactivation (Cao et al., 2024), highlighting
57 the importance of NaCl-based photochemistry in sulfate formation.

58 SSA can frequently mix with organic matter through processes such as sea-to-air emission,
59 photochemical oxidation and atmospheric transport (Liu et al., 2023b). Previous studies have
60 observed elevated sulfate concentrations in coastal regions when air masses passed through
61 inland areas due to intensive BB or other anthropogenic emissions, suggesting the possible
62 interactions between the SSA (primarily sodium chloride) and anthropogenic emissions (Qiu et
63 al., 2019; Huang et al., 2018; Wu et al., 2022). Van Pinxteren et al. (2015) observed an increase
64 in sulfate concentration (2.26 μg m⁻³) during the RV MARIA S cruise as it approached the
65 African mainland, in contrast to the marine-origin aerosol (1.59 μg m⁻³), showing significant
66 influence of BB. Hence, mixing of sea-salt and biomass burning aerosols can happen in coastal
67 regions.

68 Since the sulfate formation rate depends on the intrinsic properties of the solution matrix and
69 the two main reaction matrixes in marine boundary layer (MBL) were wet aerosol (droplet in
70 our case) and cloud/fog (bulk aqueous), both droplet and aqueous reactions are relevant for
71 studying the aqueous reactions in aerosols and clouds within MBL (Ruiz-Lopez et al., 2020;
72 Herrmann, 2003). Typically, droplet experiments were characterized by high ionic strength (up
73 to >10 M), low liquid water content (10⁻⁷-10⁻³ cm³ m⁻³) and high surface-to-volume ratio
74 whereas aqueous reactions exhibit the opposite characteristics. Additionally, droplet
75 experiments can encompass certain interfacial reaction pathways that may occur in atmospheric
76 conditions. Transmission electron microscopy (TEM) studies indicate that most coastal

77 particles are internally mixed, showing a higher proportion of organic and salt mixtures in the
78 presence of biomass burning aerosols, accompanied by an increase in sulfate (Dang et al., 2022;
79 Li et al., 2003). However, discrepancies persist between modeled simulations and measured
80 sulfate concentrations in MBL (Yu et al., 2023). The interactions of sea-salt and BB aerosols,
81 especially in multiphase reactions, can potentially unravel the intricate chemistry of sulfate
82 formation in BB affected MBL. Hence, internal mixtures of inorganic salt and water-soluble
83 organic carbons are often used in reaction studies (Tan et al., 2024).

84 In this study, we performed in-situ droplet and aqueous experiments using BB extracts-NaCl
85 mixture to explore the possible interplay between biomass burning and marine aerosols in
86 coastal areas. BB was derived from the burning of rice straw (RS), wheat straw (WS), and corn
87 straw (CS) as well as incense burning (IS). The aims of this study are to: (i) compare the
88 differences in sulfate formation among different kinds of BB-NaCl particles and BB extracts;
89 (ii) examine the impacts of the atmospheric aging ($\text{OH}\cdot$ aging) on sulfate formation across
90 different BB-NaCl particles and BB extracts; (iii) investigate the role of chloride ions in BB
91 extracts mediated sulfate formation.

92 **2 Material and methods**

93 **2.1 Burning experiments**

94 Three types of commonly used biomass (RS, WS and CS) were cut into small, uniform pieces
95 (~10 cm in length) and dried. About 100 g of the dried biomass materials (~10% moisture
96 content) was then introduced into a traditional iron stove commonly used in rural areas (Figure
97 S1). The stove was covered with a hood and the biomass was ignited using a propane lighter.
98 The generated BB smoke was collected onto 90-mm quartz filters at $0.9 \text{ m}^3 \text{ min}^{-1}$ for 10 minutes
99 by a custom-made aerosol sampler under mixed combustion conditions (include flaming and
100 smoldering, modified combustion efficiency MCE, $0.85 \leq \Delta[\text{CO}_2]/(\Delta[\text{CO}_2] + \Delta[\text{CO}]) \leq 0.95$)
101 (Ting et al., 2018). The sampler was placed 1 meter above the ground and connected to a $\text{PM}_{2.5}$
102 sampling head through a sampling pump. For incense burning (IS), laboratory-generated
103 smoldering smoke was collected on 47-mm quartz filters at a flow rate of $\sim 6.0 \text{ L min}^{-1}$ for 80
104 min using a stainless-steel combustion chamber. Note that the different combustion modes of
105 IS and BB are intentionally used to represent real-world combustion conditions. Our previous
106 study demonstrated that IS was representative of BB based on GC×GC chromatograms and
107 pixel-based partial least squares discriminant analysis (Tang et al., 2023). Hereafter, we will
108 use BB to represent both the real BB materials and the surrogate materials (IS) unless otherwise
109 specified. After sampling, the collected BB samples (fresh BB) were wrapped by pre-baked
110 aluminum foil (550 °C for 6 h) and stored at -20 °C until further analysis.

111 To achieve atmospheric $\text{OH}\cdot$ aging, the collected fresh BB filter samples were placed in a pre-
112 flushed combustion chamber (zero air, more than 24 h) and illuminated with UV lamps for 40
113 min. We used lamps of 185 nm and 254 nm, the combination of which has been widely used in
114 oxidation flow reactor design and experiments for mimicking atmospheric $\text{OH}\cdot$ concentrations
115 (Peng and Jimenez, 2020; Rowe et al., 2020; Tkacik et al., 2014; Hu et al., 2022). The estimated
116 OH exposure was $\sim 2.0 \times 10^{12} \text{ molecules cm}^{-3} \text{ s}$, equivalent to an atmospheric aging period of
117 15 days (assuming an average atmospheric OH concentration of $1.5 \times 10^6 \text{ molecules cm}^{-3}$) (Mao

118 et al., 2009). Detailed characterization of the OH exposure can be found in our previous study
119 (Tang et al., 2023).

120 **2.2 Materials and instrumentation**

121 Aqueous stock solutions of BB samples were prepared by dissolving the collected filters in
122 ultrapure water and subjecting them to ultrasonication in a cooled-water bath three times, each
123 for 20 minutes. The resulting water extracts of the BB were then filtered through 0.22 μm PTFE
124 filters and stored in brown vials at 4°C in a refrigerator. The anions, i.e., chloride, sulfate and
125 nitrate of the BB extracts were analyzed by Dionex ion chromatography (ICS 1100, CA). An
126 aliquot (~0.5 ml) of the BB or IS extracts was used for water-soluble organics detection by
127 ultra-high performance liquid chromatography (Thermo Scientific Dionex UltiMate 3000
128 UHPLC) coupled with high-resolution Orbitrap Fusion Lumos Tribrid mass spectrometry
129 (Orbitrap HRMS, Thermo Fisher Scientific, USA). The particulate organic matter was also
130 characterized by a thermal desorption module (TDS3, Gerstel) coupled to comprehensive two-
131 dimensional gas chromatography-mass spectrometer (GCMS-TQ™8050 NX, Shimadzu,
132 Japan). UV-Vis spectrometry (UV-3600, Shimadzu, Japan) was employed to examine the
133 absorbance of BB extracts. Total organic carbon (TOC) was measured by total carbon analyzer
134 (TOC-L CPH, Shimadzu, Japan). Metal concentrations were measured by inductively coupled
135 plasma-mass spectrometry (ICP-MS, Agilent 7800). Detailed analysis can be found in Text S1.
136 Aqueous stock solution of sodium chloride ($\geq 99.8\%$, Unichem) was prepared by dissolving the
137 corresponding salt in ultrapure water to obtain a concentration of 1M. The study utilized high
138 purity grade synthetic air and nitrogen supplied by the Linde HKO Ltd., while sulfur dioxide
139 was obtained from the Scientific Gas Engineering Co., Ltd.

140 **2.3 Multiphase and aqueous-phase reactions of S(IV)**

141 In SO_2 uptake experiments, the stock solution of BB extracts was premixed with sodium
142 chloride solution (1M) at a volume ratio of 1:1 and the solutions had pH a of 4-6. A droplet
143 generator (Model 201, Uni-Photon Inc.) was then utilized to deposit droplets onto a
144 hydrophobic substrate (model 5793, YSI Inc.) for SO_2 uptake experiments. Reactive SO_2 uptake
145 experiments were performed via a flow cell/in-situ Raman system at controlled room
146 temperature (23-25°C). The top and bottom quartz windows of the flow cell were used for
147 Raman analysis and UV irradiation, respectively. The light experiment was performed using a
148 xenon lamp (model 6258, ozone free, 300W, Newport, light intensity of 1318 mW/cm^2), with
149 photon flux of 9.8×10^{15} photons $\text{cm}^{-2} \text{ s}^{-1}$ in 280-420 nm received by particles in the flow cell
150 (Zhang and Chan, 2023b). Identical experiments were conducted in the dark, with the lights off
151 and the experimental area kept in complete darkness. The relative humidity (RH) inside the
152 flow cell was adjusted to 80% by mixing dry and wet synthetic air or nitrogen. The particles
153 were then equilibrated at 80% RH for over 60 min and remained liquid throughout the
154 experiment period. SO_2 was introduced into the system to reach a concentration of 8.0 ppm.
155 The prescribed size used in our in-situ Raman research was $60 \pm 5 \mu\text{m}$. Despite using particles
156 for droplet experiments that were larger than ambient fine particles, we employed the SO_2
157 uptake coefficient (γ_{SO_2}) as a kinetic parameter to account for the particle size effects.
158 Comprehensive calculation of γ_{SO_2} can be found in our previous studies (Gen et al., 2019a, b;
159 Tang et al., 2023; Zhang et al., 2020a).

160 Aqueous-phase photochemical reactions were performed using a custom-built quartz photo
161 reactor (Mabato et al., 2023; 2022). Specifically, a 500 mL solution containing 100 ppm
162 bisulfite and 1 ppm BB TOC extracts were continuously mixed using a magnetic stirrer
163 throughout the experiments. Note that the 1 ppm BB TOC and 100 ppm bisulfite align well
164 with the atmospheric-relevant ranges in aqueous aerosols, fogs and clouds, where PS
165 concentration can reach hundreds of micromolar and total sulfur concentration can exceed
166 several millimolar (Anastasio et al., 1997; Guo et al., 2012; Shen et al., 2012; Rao and Collett,
167 1995). To achieve air-saturated conditions, synthetic air was continuously introduced to the
168 solutions at a flow rate 0.5 L min^{-1} throughout the experiments. The above mixed solutions were
169 then exposed to radiation via the same xenon lamp as in the droplet experiments. Samples were
170 collected at 1h interval for a total of 8 h for sulfate and bisulfite analysis using ion
171 chromatography.

172

173 **3 Results and Discussion**

174 **3.1 Enhanced sulfate production of BB-NaCl droplets compared to IS-NaCl droplets.**

175 As no sulfate was detected in the dark conditions for any of the experiments, we have focused
176 on the light experiments. Figure 1 depicts the sulfate production by (a) fresh BB-NaCl; (b) aged
177 BB-NaCl droplets as a function of time in the presence of light, air and SO_2 at 80% RH. As our
178 previous study (Tang et al., 2023) has found significantly higher sulfate formation of IS-NaCl
179 droplets over NaCl droplets, here we only focus on the comparison of sulfate formation between
180 different kinds of BB-NaCl droplets and IS-NaCl droplets. Regardless of whether the extracts
181 were fresh or aged, the sulfate production by real BB-NaCl droplets was higher than IS-NaCl
182 droplets. Specifically, sulfate formed by fresh (F) BB-NaCl droplets followed the trends of $\text{CS}_F\text{-NaCl}$
183 $(16.8 \pm 2.6 \text{ mM ppmC}^{-1}) > \text{RS}_F\text{-NaCl}$ $(9.8 \pm 0.1 \text{ mM ppmC}^{-1}) > \text{WS}_F\text{-NaCl}$ $(4.2 \pm 0.2 \text{ mM}$
184 $\text{ppmC}^{-1}) > \text{IS}_F\text{-NaCl}$ $(0.8 \text{ mM ppmC}^{-1})$ after illumination for 1080 min. In aged (A) samples,
185 while $\text{BB}_A\text{-NaCl}$ is more efficient than $\text{IS}_A\text{-NaCl}$ in sulfate formation, the order of sulfate
186 formation was different from the fresh samples: $\text{RS}_A\text{-NaCl}$ $(35.2 \pm 0.6 \text{ mM ppmC}^{-1}) > \text{CS}_A\text{-}$
187 NaCl $(13.0 \pm 0.1 \text{ mM ppmC}^{-1}) > \text{WS}_A\text{-NaCl}$ $(6.0 \pm 1.6 \text{ mM ppmC}^{-1}) > \text{IS}_A\text{-NaCl}$ $(0.6 \text{ mM}$
188 $\text{ppmC}^{-1})$. The sulfate enhancement factors of $\text{RS}_F\text{-NaCl}$, $\text{WS}_F\text{-NaCl}$, and $\text{CS}_F\text{-NaCl}$ over $\text{IS}_F\text{-}$
189 NaCl after 18 h SO_2 uptake ($\text{Sulfate}_{\text{BB}_F\text{-NaCl}/\text{IS}_F\text{-NaCl}}$) were 11.7, 5.0 and 20.0, respectively.
190 The enhancement of sulfate can also be observed in aged BB samples, with values of 54.3, 9.2
191 and 20.1 for $\text{RS}_A\text{-NaCl}$, $\text{WS}_A\text{-NaCl}$, and $\text{CS}_A\text{-NaCl}$, respectively. The lower sulfate formation
192 of IS-NaCl droplets than BB-NaCl droplets can be explained by the significantly higher TOC
193 concentration of IS due to the incomplete and smoldering combustion (Table S1). The TOC
194 concentration of the IS extracts ($>550 \text{ mg L}^{-1}$) was nearly an order of magnitude higher than
195 that of the BB extracts ($34.0\text{-}69.9 \text{ mg L}^{-1}$), while $\text{WSOC}/(\text{WSOC} + \sum \text{anions})$ exhibited a more
196 than tenfold increase in BB extracts than in IS extracts. Previous studies have confirmed that
197 the smoldering condition of BB will result in significantly more organic compounds and less
198 ions than flaming condition (Wang et al., 2020b; Fushimi et al., 2017; Kalogridis et al., 2018;
199 Kim et al., 2018). Additionally, significantly higher polycyclic aromatic hydrocarbons (PAHs)
200 proportion (12.2%-16.6% by intensity) than IS ($\sim 5.0\%$) were observed by GC \times GC-MS. Huang
201 et al. (2022a) reported higher PAHs in BB particulates (CS, WS, RS, $>262.5 \text{ mg kg}^{-1}$, $>3.7\%$ of

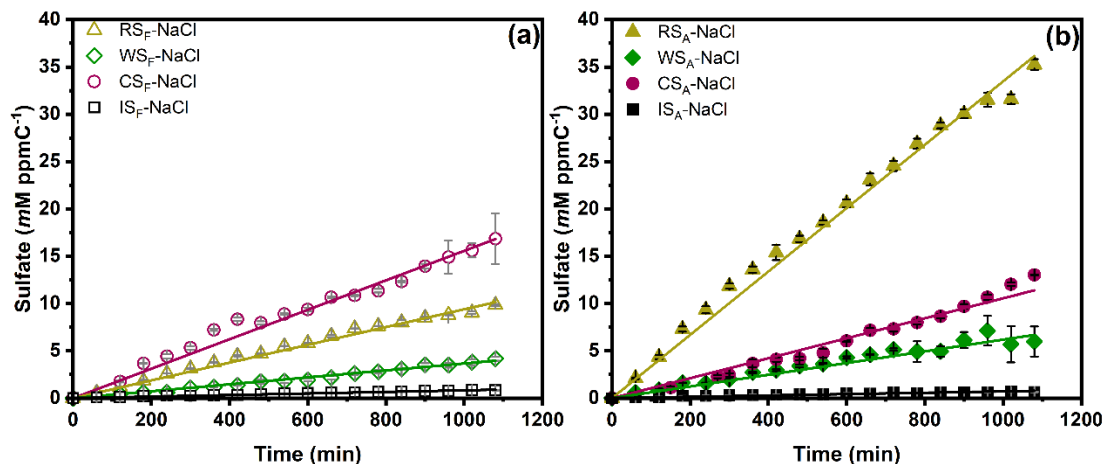
202 organic matter) than in IS particulates (3.3 mg kg^{-1} , 0.9% of organic matter) (Song et al., 2023).
203 Fushimi et al. (2017) and Kim et al. (2021) demonstrated that more PAHs would be emitted
204 under flaming compared to smoldering conditions. PAHs like pyrene, fluoranthene, and
205 phenanthrene have been recognized as PS (Jiang et al., 2021; Yang et al., 2021) and are mainly
206 from combustion processes, e.g., pyrosynthesis from aliphatic and aromatic precursors in
207 biomass burning processes and the constituents vary with temperatures and oxygen contents
208 (Pozzoli et al., 2004). The higher percentage of PAHs in BB together with the collection
209 procedure (mixed combustion and higher temperature for real BB while smoldering and lower
210 temperature for IS) suggested the BB materials would generate more PAHs at high temperatures
211 and may contribute to sulfate formation.

212 Table 1 and Figure S2 presents the reactive (γ_{SO_2}) and normalized reactive SO_2 uptake
213 coefficients ($n\gamma_{SO_2}$) of different BB-NaCl droplets. The γ_{SO_2} obtained in our study are $0.9 -$
214 6.6×10^{-6} , which are consistent but fall on the low side of the reported heterogeneous SO_2
215 oxidation processes, including nitrate photolysis ($10^{-6}-10^{-5}$) (Gen et al., 2019a), TMI-catalyzed
216 oxidation ($10^{-6}-10^{-4}$) (Zhang et al., 2024), NO_2/O_3 oxidation ($10^{-6}-10^{-4}$) (Zhang et al., 2021a;
217 Zhang and Chan, 2023a) and peroxide oxidation ($10^{-6}-10^{-1}$) (Wang et al., 2021a; Ye et al., 2018;
218 Yao et al., 2019). Additionally, the reported γ_{SO_2} in our study aligns well with the results
219 obtained from ambient samples in Beijing (Zhang et al., 2020b). The large discrepancy of the
220 reported γ_{SO_2} can be attributed to the differences in aerosol components, particle size, RH, SO_2
221 and oxidants concentrations. From our results, it appears that sulfate formation from BB-NaCl
222 particles is much less effective than particles under nitrate photolysis. It is interesting to note
223 that Zhou et al. (2023) found particles coated with model PS compounds much more effective
224 in sulfate formation than nitrate particles under photolysis in a PAM reactor. The much shorter
225 residence time in that reactor (2.5 min) and higher PS concentration ($\sim 66 \text{ mM}$) than the
226 exposure time of filter samples (40 min) and PS concentration ($< 250 \text{ ppm}$) in our sulfate
227 experiments may explain the differences in the comparison of PS/BB and nitrate photolysis
228 results. Higher $n\gamma_{SO_2}$ were found for fresh and aged real BB-NaCl than IS-NaCl droplets,
229 following the trend of : $CS_F\text{-NaCl}$ ($8.8 \times 10^{-8} \text{ ppmC}^{-1}$) $>$ $RS_F\text{-NaCl}$ ($6.2 \times 10^{-8} \text{ ppmC}^{-1}$) $>$ $WS_F\text{-NaCl}$
230 ($2.0 \times 10^{-8} \text{ ppmC}^{-1}$) $>$ $IS_F\text{-NaCl}$ ($0.61 \times 10^{-8} \text{ ppmC}^{-1}$) and $RS_A\text{-NaCl}$ ($2.2 \times 10^{-7} \text{ ppmC}^{-1}$) $>$ $CS_A\text{-NaCl}$
231 ($6.2 \times 10^{-8} \text{ ppmC}^{-1}$) $>$ $WS_A\text{-NaCl}$ ($3.5 \times 10^{-8} \text{ ppmC}^{-1}$) $>$ $IS_A\text{-NaCl}$ ($0.46 \times 10^{-8} \text{ ppmC}^{-1}$), respectively.

232 In our previous study, we observed a significant increase in sulfate formation for IS-NaCl
233 droplets than NaCl droplets, which we attributed to photosensitization (Tang et al., 2023).
234 Considering the fact that BB-NaCl droplets produced sulfate more efficiently than IS-NaCl
235 droplets and NaCl droplets, we explore the underlying mechanisms driving this phenomenon.
236 Possible reasons include nitrate (from BB extracts or newly formed) photolysis, $[Cl^- - H_3O^+ - O_2]$
237 photoexcitation (Cl^- from BB extracts), H_2O_2 oxidation, BC-catalyzed oxidation, reactive
238 nitrogen species oxidation, and organics-driven pathways e.g., HCHO, photosensitizing
239 components, organic peroxide, and TMI-organic oxidation (Ye et al., 2023).

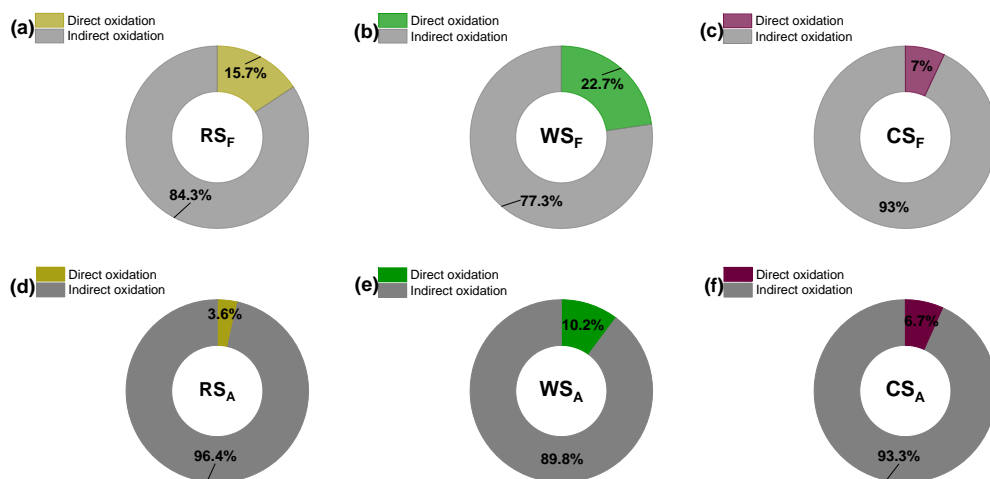
240 Since there was no nitrate peak in our Raman spectra in all experiments, the potential impact
241 from nitrate photolysis was excluded. Besides, the significantly low Cl^- concentration (0.0002-
242 0.001M) in the original BB extracts (compared to 1M NaCl, Table S1) has minimized the
243 influence of chloride photoexcitation of $[Cl^- - H_3O^+ - O_2]$ (Cl^- from BB extracts) on the sulfate

244 formation. Reactive nitrogen species e.g., NO_x, HONO and NH₃ were neither introduced nor
245 detected in our system, indicating that the oxidation pathway involving reactive nitrogen
246 species was insignificant. Additionally, the water extraction process has excluded the possibility
247 of BC-catalyzed oxidation. The absence of sulfate formation in dark conditions ruled out the
248 involvement of direct H₂O₂ oxidation and organic peroxide oxidation pathways. The
249 concentrations of TMI did not exhibit a consistent relationship with the sulfate formation
250 observed in both BB_F-NaCl and BB_A-NaCl droplets (Figure S3), suggesting that the TMI-
251 catalyzed oxidation pathway may not be responsible for the observed phenomenon. Therefore,
252 the most probable reason for the enhancement of sulfate formation by BB-NaCl droplets over
253 NaCl droplets would be the photosensitizing components. Given the complexity and the lack
254 of a method to quantify PS in BB aerosols, using the total TOC concentration as an upper limit
255 for estimating PS concentration is considered a compromise that allows for systematic
256 comparison. Our goal is to compare the photosensitizing ability in different chemical systems,
257 but not to quantify their absolute values. Therefore, the sulfate formation reported here can be
258 considered as the lower limit of photosensitizing capacity. State-of-the-art mass spectrometry
259 analysis including UHPLC-Orbitrap-MS and GC×GC-MS showed the existence of possible PS
260 such as PAHs (e.g., fluoranthene, pyrene, cyclopenta[cd]pyrene, 4-methylphenanthrene,
261 benzo[a]pyrene, perylene, Table S2) and aromatic carbonyls (SyrAld, VL, 3,4-
262 dimethoxybenzaldehyde, acetophenone, acetosyringone, Table S2). Photosensitizing
263 components can directly or indirectly (by forming secondary oxidants in the presence of oxygen)
264 oxidize S(IV) to S(VI). Wang et al. (2020a) proposed a direct oxidation process of S(IV) to
265 sulfate by excited triplet states of photosensitizers (³PS*). To explore the contribution of the
266 direct ³PS* oxidation on sulfate formation, we performed the same sets of experiments in N₂-
267 saturated condition, shown in Figure 2. Under N₂-saturated conditions, secondary oxidants such
268 as HO₂•, OH• oxidation pathway can be ruled out due to the lack of oxygen. Despite initial
269 molecular oxygen in the droplets may also participate in sulfate formation under N₂-saturated
270 conditions, its contributions are likely minimal. Consequently, the sulfate formed under N₂-
271 saturated condition can be considered as the upper limit of direct ³PS* oxidation. The BB-NaCl
272 droplets showed only direct PS* oxidation contribution of 3.6% to 22.7%, highlighting the
273 predominant role of secondary oxidants (Tang et al., 2023). For BB_F-NaCl droplets, the
274 contribution of direct ³PS* followed the trend of WS_F-NaCl (22.7%) > RS_F-NaCl (15.7%) >
275 CS_F-NaCl (7.0%), while for BB_A-NaCl droplets, WS_A-NaCl (10.2%) > CS_A-NaCl (6.7%) >
276 RS_A-NaCl (3.6%) was observed. In summary, regardless of whether fresh or aged, the
277 secondary oxidants triggered by indirect ³PS* oxidation were the main reason for sulfate
278 formation, highlighting the importance of O₂ in ³PS* mediated oxidation processes.



279

280 Figure 1. Sulfate production under different droplet compositions as a function of time by
 281 droplet experiments: (a) fresh BB-NaCl droplets; (b) aged BB-NaCl droplets in air at 80% RH.
 282 RS, WS, CS and IS represent rice straw, wheat straw, corn straw and incense burning,
 283 respectively. The subscripts F and A represent fresh and aged, respectively.



284

285 Figure 2 Contributions of direct and indirect PS* oxidation to sulfate in droplet experiments

286

287 Table 1. Sulfate formation rate constant ($k_{SO_4^{2-}}$), reactive (γ_{SO_2}) and normalized SO_2 uptake
 288 coefficient ($n\gamma_{SO_2}$) of various particle compositions at 80% RH. Sulfate formation rate ($k_{SO_4^{2-}}$)
 289 for aqueous phase reactions using different BB extracts and model compounds. 1, 10, 100 and
 290 200 represent the concentration of different compounds (in ppm).

Particle Composition	$k_{SO_4^{2-}}$ ($\mu\text{M min}^{-1} \text{ ppmC}^{-1}$)	γ_{SO_2}	$n\gamma_{SO_2}$ a ppmC ⁻¹
RS _F -NaCl	9.4 ± 0.10	$(2.2 \pm 0.023) \times 10^{-6}$	$(6.2 \pm 0.066) \times 10^{-8}$
WS _F -NaCl	3.7 ± 0.048	$(0.66 \pm 0.0086) \times 10^{-6}$	$(2.0 \pm 0.027) \times 10^{-8}$

CS _F -NaCl	15.6 ± 0.11	(2.0 ± 0.015) × 10 ⁻⁶	(8.8 ± 0.065) × 10 ⁻⁸
IS _F -NaCl	0.83 ± 0.011	(1.7 ± 0.034) × 10 ⁻⁶	(0.61 ± 0.012) × 10 ⁻⁸
RS _A -NaCl	33.5 ± 0.38	(6.6 ± 0.074) × 10 ⁻⁶	(21.5 ± 0.24) × 10 ⁻⁸
WS _A -NaCl	6.2 ± 0.18	(0.92 ± 0.027) × 10 ⁻⁶	(3.5 ± 0.10) × 10 ⁻⁸
CS _A -NaCl	10.6 ± 0.23	(1.0 ± 0.023) × 10 ⁻⁶	(6.2 ± 0.13) × 10 ⁻⁸
IS _A -NaCl	0.72 ± 0.026	(1.3 ± 0.052) × 10 ⁻⁶	(0.46 ± 0.017) × 10 ⁻⁸

Aqueous Reactions	Concentration (ppm)	$k_{so_4^{2-}}$ (ppm min ⁻¹)	$k_{so_4^{2-}}^a$ (μM min ⁻¹)
RS _F	1	0.31	3.2
RS _F -NaCl	1-100	0.16	1.6
RS _F -NaCl	1-200	0.085	0.9
WS _F	1	0.19	2.0
CS _F	1	0.25	2.6
IS _F	1	0.19	2.0
RS _A	1	0.33	3.4
RS _A -NaCl	1-100	0.37	3.8
RS _A -NaCl	1-200	0.63	6.4
WS _A	1	0.26	2.7
CS _A	1	0.33	3.4
IS _A	1	0.080	0.82
NaCl	100	0.051	0.52
NaCl	200	0.079	0.81
SyrAld	1	0.15	1.5
SyrAld-Pyz	1-1	0.68	7.1
SyrAld-Pyz-NaCl	1-1-10	0.67	6.9
SyrAld-Pyz-NaCl	1-1-100	0.55	5.7
SyrAld-Pyz-NaCl	1-1-200	0.50	5.2
SyrAld-4-NC	1-1	0.11	1.1
SyrAld-4-NC-NaCl	1-1-10	0.13	1.4
SyrAld-4-NC-	1-1-100	0.13	1.4

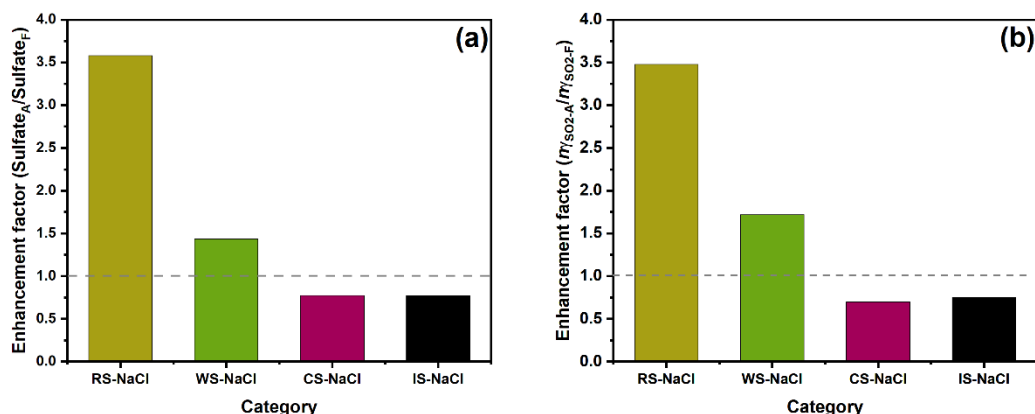
NaCl			
SyrAld-4-NC-NaCl	1-1-200	0.15	1.5
SyrAld-NaCl	1-10	0.11	1.1
SyrAld-NaCl	1-100	0.17	1.8
SyrAld-NaCl	1-200	0.17	1.7
VL	1	0.26	2.7
VL-Pyz	1-10	0.61	6.4
VL-Pyz-NaCl	1-1-10	0.55	5.8
VL-Pyz-NaCl	1-1-100	0.43	4.5
VL-Pyz-NaCl	1-1-200	0.42	4.3
VL-4-NC	1-1	0.17	1.7
VL-4-NC-NaCl	1-1-10	0.22	2.3
VL-4-NC-NaCl	1-1-100	0.27	2.7
VL-4-NC-NaCl	1-1-200	0.23	2.4
VL-NaCl	1-10	0.25	2.6
VL-NaCl	1-100	0.26	2.7
VL-NaCl	1-200	0.28	2.9

^aThe $n\gamma_{SO_2}$ was calculated by normalizing the γ_{SO_2} with the TOC concentration in the BB extracts, i.e., $n\gamma_{SO_2} = \gamma_{SO_2}/TOC$

291

292 **3.2 Aging effects on sulfate formation across various BB materials**

293 To investigate the aging effects across various BB materials, we subjected the collected BB
 294 filters to OH radical aging by irradiating them with UV lights at wavelengths of 185 nm and
 295 254 nm. This combination effectively generate OH radicals (Tang et al., 2023). Figure S4
 296 exhibits the differences in sulfate formation rates of different fresh and aged BB materials. RS
 297 and WS show sulfate formation enhancement, while CS and IS show reduction after aging.
 298 Figure 3(a) shows that the 18h sulfate enhancement factor ($Sulfate_A/Sulfate_F$) followed the trend
 299 of RS-NaCl (3.6) > WS-NaCl (1.4) > CS-NaCl (0.8) \approx IS-NaCl (0.8), which is neither consistent
 300 with the trends of sulfate formation for BB_F -NaCl nor BB_A -NaCl, indicating that aging
 301 processes have different influence on sulfate formation towards BB materials. A similar trend
 302 was found for $n\gamma_{SO_2}$, showing the highest and lowest sulfate enhancement for RS-NaCl (3.5)
 303 and IS-NaCl (0.7), respectively.



304

305 Figure 3. Enhancement factor of (a) sulfate and (b) normalized SO_2 uptake coefficient $n_{\gamma_{SO_2}}$
 306 between fresh and aged BB-NaCl droplets by droplet experiments.

307 Aqueous reactions using fresh/aged BB extracts were performed to investigate the aging effects
 308 on the sulfate formation in cloud phase (Figure S5). As the experiment proceeded, sulfate
 309 concentrations accumulated while bisulfite concentrations decreased. Concurrently, the pH of
 310 the aqueous solution decreased from approximately 5.0 to 3.0, reflecting enhanced acidity.
 311 Lower sulfate formation rates were observed for bulk reactions compared to droplets reactions,
 312 which may be attributed to the accelerated reactions induced by PS at the air-water interface
 313 (Wang et al., 2024c; Martins-Costa et al., 2022), as well as differences in concentrations of
 314 S(IV) and NaCl. However, given that interfacial reactions are closely linked to particle size
 315 (Wei et al., 2020; Chen et al., 2022b), and additional research is needed to better understand its
 316 influence. Our experiments involve large droplets of the size of 60 μm . The interfacial effects
 317 of such large droplets may not be evident. Future work should use submicron and nanometer
 318 size particles to examine the interfacial effects. In bulk experiments, all BB extracts have higher
 319 $k_{SO_4^{2-}}$ after aging. The increased sulfate formation of BB extracts after aging may be due to
 320 changes in their chemical compositions. Compared to RS_F (28.3% for CHON- and 67.3% for
 321 CHN+ in total intensity), RS_A has higher CHON- (36.1%) and CHN+ (88.3%) percentages (Figs.
 322 S6-S7). Zhao et al. (2022) observed a slight increase in CHON percentage for RS from 53.4%
 323 to 56.2% after aging. Similar trend was observed for CS extracts, where CHON- and CHN+
 324 percentage increases from 26.7% and 65.2% to 31.5% and 68.8%, respectively, after aging.
 325 Given the presence of chromophoric compounds in BrC (Laskin et al., 2015), we constrained
 326 the DBE values to the range of $0.5C \leq DBE \leq 0.9C$ to semi-qualitatively distinguish BrC
 327 chromophores in the dissolved organic carbon (Lin et al., 2018). $BB_{F/A}$ was defined as the water-
 328 soluble organic species while $BB_{F/A-BrC}$ represented the molecularly identified water-soluble
 329 brown carbon falling in the range of $0.5C \leq DBE \leq 0.9C$ in BB extracts. These definitions will
 330 be consistently applied hereafter. Higher amounts of CHON- species were found in RS_{A-BrC}
 331 (41.9%) and CS_{A-BrC} (35.5%) than RS_{F-BrC} (32.3%) and CS_{F-BrC} (34.7%). One of the key
 332 categories of CHON- is nitrated aromatics, which have been widely identified in lab-generated
 333 BB smoke (Huang et al., 2022b; Wang et al., 2017a; Zhang et al., 2022; Xie et al., 2019) and
 334 field campaigns (Salvador et al., 2020; Mohr et al., 2013; Chen et al., 2022a). A series of
 335 CHON- species, e.g., $C_6H_5NO_3$, $C_6H_5NO_4$, $C_7H_7NO_3$, and $C_8H_9NO_3$, which were tentatively
 336 identified as nitrophenol, nitrocatechol, methyl-nitrophenol, and dimethyl-nitrophenol, have

337 been detected in our BB extracts. Nitrophenols photolysis has been found to be a potential
338 source of OH radicals (Sangwan and Zhu, 2018; Guo and Li, 2023; Cheng et al., 2009; Sangwan
339 and Zhu, 2016). Therefore, the increase in sulfate formation by RS_A and CS_A may partially be
340 related to the more oxidants generated by nitrophenol photolysis.

341 Approximately 80% of the CHN^+ species identified exhibited a diatomic nitrogen composition
342 in their molecular formula. The precise determination of the molecular structures of these
343 compounds solely based on elemental composition is challenging due to the presence of stable
344 isomers. However, the N-bases, which contain two nitrogen atoms, can be attributed to various
345 N-heterocyclic alkaloids (Figure S8). For example, homologs of $C_5H_6N_2(CH_2)_n$ were likely
346 pyrazine, pyrimidine or amino pyridine, which were composed of six-membered heterocyclic
347 rings with N atoms and alkyl side chains (Lin et al., 2012; Laskin et al., 2009). $C_5H_8N_2(CH_2)_n$
348 were likely alkyl-substituted imidazole compounds, featuring a five-membered heterocyclic
349 ring with two nitrogen atoms as the core structure and alkyl side chains (Lin et al., 2012; Laskin
350 et al., 2009). For $C_7H_6N_2(CH_2)_n$ homologs, the core skeleton was $C_7H_6N_2$, with an AI_{mod} of 0.8,
351 indicating its distinctive characteristics of compounds containing fused five-membered and six-
352 membered rings, such as benzimidazole or indazole (Wang et al., 2017b). Redox-inactive
353 heterocyclic nitrogen-containing bases, e.g., pyridine, imidazole, and their derivatives, have
354 been shown to enhance the redox activity of humic-like substances (HULIS) fraction by
355 hydrogen-atom transfer, with the degree of enhancement directly correlated to their
356 concentration (Dou et al., 2015; Kipp et al., 2004). Thus, the increased CHN^+ percentage may
357 also contribute to the enhanced sulfate formation of RS_A and CS_A by acting as a H-bond
358 acceptor to facilitate the $^3PS^*$ -mediated oxidation by generating more oxidants.

359 However, the $CHON^-$ and CHN^+ percentages in WS_A were lower than WS_F , indicating that the
360 sulfate enhancement in WS_A was not due to the $CHON^-$ and CHN^+ species. Instead, CHO^-
361 accounted for higher proportion in WS_A (68.5%) and WS_{A-BrC} (68.9%) than WS_F (65.0%) and
362 WS_{F-BrC} (64.8%). This aligns with a prior AMS study, showing increased CHO^- proportions in
363 aged wheat burning emissions (Fang et al., 2017). We suppose that CHO^- compounds,
364 particularly photosensitizing compounds with carbonyl groups, would explain the difference of
365 sulfate formation in WS extracts (Gómez Alvarez et al., 2012; Mabato et al., 2023; Felber et al.,
366 2020; Fu et al., 2015). Therefore, we filtered the chemical formula of CHO^- species from
367 UHPLC-Orbitrap-HRMS by applying the maximum carbonyl ratio (MCR) (Zhang et al., 2021b;
368 Wang et al., 2024a; Calderon-Arrieta et al., 2024; Liu et al., 2023a), H/C , O/C as well as
369 modified aromaticity index (AI_{mod}) to focus on potential PS (Zherebker et al., 2022; Koch and
370 Dittmar, 2006). In short, molecular formula were classified into six groups, namely, condensed
371 aromatics ($AI_{mod} \geq 0.67$), polyphenolics ($0.50 < AI_{mod} < 0.67$), highly unsaturated and phenolic
372 compounds ($AI_{mod} \leq 0.5$, $H/C < 1.5$), aliphatics ($H/C \geq 1.5$, $O/C \leq 0.9$, $N=0$), peptide-like
373 compounds ($H/C \geq 1.5$, $O/C \leq 0.9$, $N > 0$) and sugar-like compounds ($H/C \geq 1.5$, $O/C > 0.9$), details
374 can be found in Text S1. As aliphatics, peptide-like compounds and sugar-like compounds are
375 unlikely to be PS, we exclude them as potential PS. By applying a data filtration process
376 involving CHO^- , condensed aromatics, polyphenolics, highly unsaturated and phenolic
377 compounds based on the aforementioned criteria, as well as $MCR \geq 0.9$ (which includes oxidized
378 unsaturated and highly unsaturated compounds such as PS like imidazole-carboxaldehyde and
379 PAHs) (Zhang et al., 2021b), 52.6% and 49.7% of the compounds (by intensity) can be

380 considered as potential PS in WS_A and WS_F , respectively. The main compositional difference
381 lies in polyphenolics, comprising 26.3% and 21.8% of WS_A and WS_F respectively. Therefore,
382 the higher sulfate formation in WS_A may be related to the higher contributions of the
383 polyphenolics, e.g., $C_8H_8O_3$.

384 To summarize, we propose that the enhanced sulfate formation in CS_A and RS_A was likely due
385 to the increased proportions (by intensity) of CHON and CHN species, potentially nitrophenols
386 and N-heterocyclic compounds. Conversely, the increased sulfate formation in WS_A appears to
387 be linked to a higher percentage of CHO species. However, the associations between detailed
388 chemical characteristics and sulfate formation were not provided in this study due to the
389 complexity of the interactions between different chemical categories and difficulties in the
390 interpretation of the coefficients. Future studies are needed to elucidate the relationships
391 between sulfate formation and the chemical characteristics.

392 3.3 Effects of Chloride and Nitrogen-containing Species on Sulfate Formation

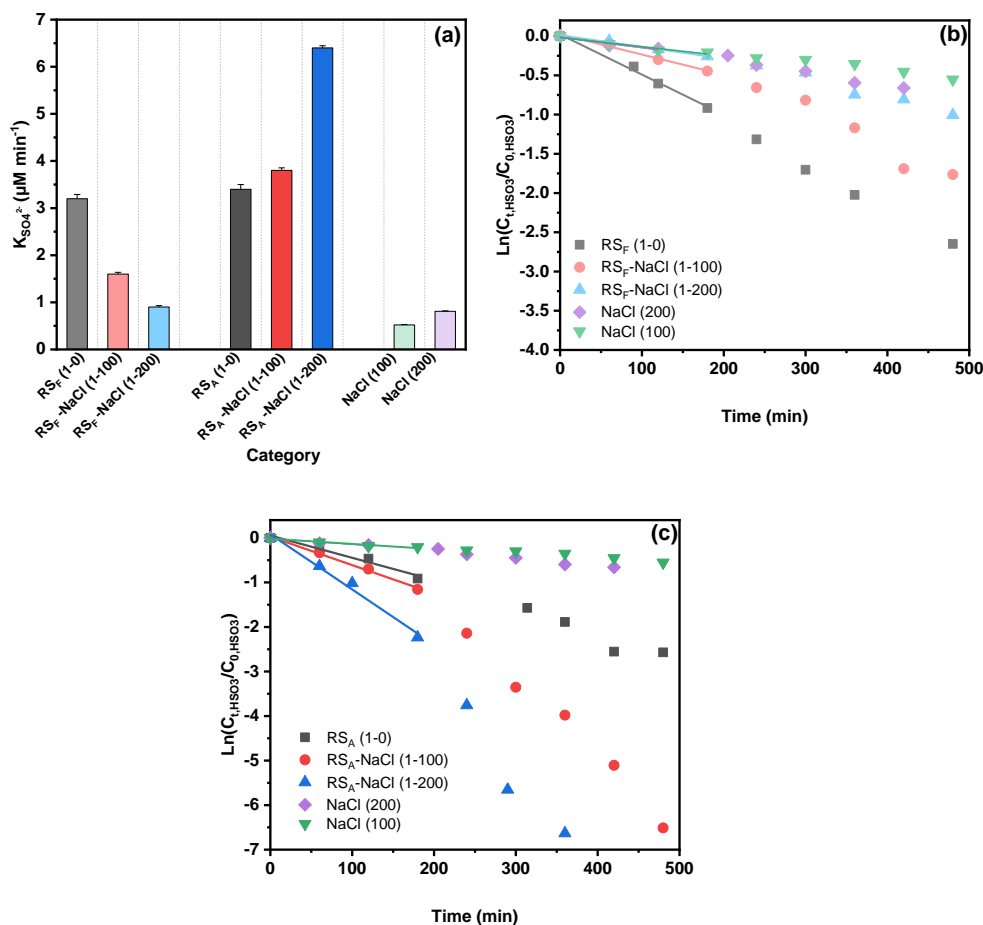
393 Unlike the droplet experiments where RS-NaCl has the highest sulfate enhancement factor after
394 aging, aqueous reaction results (without NaCl) show a sulfate enhancement trend of
395 $WS > CS > RS > IS$, suggesting that chloride may take effect in the droplet experiments, especially
396 in RS-NaCl system. Therefore, bulk reaction experiments using RS extracts as an example were
397 performed with 100-200 ppm NaCl additions, where the NaCl to TOC ratio ranged from 100:1
398 to 200:1 to match the 100:1 to 1000:1 range in droplet experiments, in order to evaluate the
399 effects of chloride on sulfate formation. Interestingly, incorporating NaCl yielded contrasting
400 results for RS_F and RS_A (Figure 4). While the addition of NaCl enhanced sulfate formation in
401 RS_A , it showed the opposite trend in RS_F . The nature of the cations and ionic strength may
402 affect the sulfate formation rate; however, previous studies have indicated that their effects are
403 negligible (Zhang and Chan, 2024; Parker and Mitch, 2016). The opposite effect of the NaCl
404 addition on RS_F and RS_A , to some extent, explains the significantly higher sulfate and SO_2
405 uptake coefficient enhancement factor for RS-NaCl in Fig. 2. Compared to the RS-based system,
406 NaCl control experiment showed minimum (but non-zero) sulfate formation (Table 1 and
407 Figure 4). On one hand, it supported the findings that chloride participated in the sulfate
408 formation under light but no sulfate formation under dark (Cao et al., 2024; Tang et al., 2023;
409 Zhang and Chan, 2024). On the other hand, the opposite trend of Cl^- effects on RS_F and RS_A
410 reflects its complex interactions with BB extracts under light and air. While direct reaction
411 between S(IV) species and $^3PS^*$ may occur (Wang et al., 2020a), other pathways, i.e.,
412 interactions among halide ions, PS and oxygen should also be considered. PS in BB extracts
413 can absorb solar radiation and form $^3PS^*$, which can then react with molecular oxygen and form
414 singlet-state oxygen $^1O_2^*$ through energy transfer. $^3PS^*$ can also react with H-donor, typically
415 organic acids (RH, e.g., vanillic acid, succinic acid, azelaic acid, glutaric acid, sorbic acid,
416 salicylic acid, Table S3) through H transfer reactions, and form a ketyl radical (PSH•) and an
417 alkyl or phenoxy radical (R•). PSH• and R• can then participate in a series of reactions to form
418 $OH•$, $HO_2•$, H_2O_2 and $O_2•^-$. In the presence of a large excess of Cl^- , Cl^- can act as an electron
419 donor, and react with $^3PS^*$, forming a $Cl•$ and a deprotonated ketyl radical (PS•) (Jammoul et
420 al., 2009). Further reactions are similar to the abovementioned reactions, including the
421 formation of reactive chlorine species (RCS, i.e., $Cl•$, $Cl_2•^-$ and $ClOH•^-$) and reactive oxygen

422 species (ROS, i.e., OH•, HO₂•, H₂O₂ and O₂•⁻). These RCS and ROS simultaneously contribute
423 to S(IV) oxidation to S(VI) (Zhang and Chan, 2024).

424 Statistical analysis using the Spearman correlation coefficients, as guided by the Shapiro-Wilk
425 test (Table S4), revealed that the CHO, CHON, and CHN species exhibited significant
426 correlations ($|R| > 0.7$) with the sulfate formation rate ($p < 0.01$, Figure S9). As PS can be the
427 main CHO species contributing to sulfate formation, N-containing organic compounds (NOCs),
428 i.e., CHN and CHON species, may affect the chloride contribution on sulfate formation rate.
429 Therefore, we selected SyrAld and VL as model CHO (PS), pyrazine (Pyz) as a model CHN,
430 and 4-nitrocatechol (4-NC) as a model CHON to elucidate how potential chemical compounds
431 can alter the effects of chloride on sulfate formation rate by studying the CHO+Cl⁻,
432 CHO+CHN+Cl⁻, and CHO+CHON+Cl⁻ systems. For SyrAld and VL, as the [Cl⁻]₀/[PS]₀
433 increases, $k_{SO_4^{2-}}$ initially decreases and then increases. The initial decrease of $k_{SO_4^{2-}}$ may be
434 attributed to the quenching of ³PS* by electron transfer from Cl⁻ or loss of OH radicals by
435 forming ClOH• through reaction of OH•+Cl⁻ ↔ ClOH• (Anastasio and Newberg, 2007).
436 Excessive chloride (e.g. 100 and 200 ppm) may generate Cl and OH radicals through
437 photoexcitation in the presence of air and water and compensate for the loss of ³PS* or OH
438 radicals. Previous studies have shown controversial influence of halides on the photosensitized
439 oxidation of organic compounds or bisulfite. Parker and Mitch (2016) and Zhang et al. (2023)
440 attributed the significantly higher photodegradation of dienes, thioethers and acetaminophen to
441 the formation of reactive halogen species generated by the reactions of PS and halides. Zhang
442 and Chan (2024) reported that [Cl⁻/PS]₀ in the range of 1:2 to 4:1 did not lead to significant
443 difference in sulfate formation, possibly due to the insufficient Cl⁻ concentration in triggering
444 the interplay between PS and Cl⁻. The differences between the current results and the
445 aforementioned study might be attributed to the higher [Cl⁻/PS]₀ (up to 1:200) which may have
446 been sufficient to initiate the relevant reactions, as well as the difference in photosensitizing
447 capacities of the PS studied (triplet quantum yield of 0.86 ± 0.05 for 2-IC and 0.21 ± 0.01 for
448 VL) (Felber et al., 2021; 2020). Safiarian et al. (2023) reported that increasing chloride
449 concentrations facilitated anthracene photosensitization by producing high-level reactive
450 oxygen species (ROS). Wang et al. (2023a) found that the effects of chloride on sulfate
451 formation depended on the specific PS: enhancing sulfate production for benzophenone (BP)
452 and 3,4-dimethoxybenzaldehyde (DMB), but decreasing it for 1,4-naphthoquinone.

453 When incorporating CHN species, a 2-3-fold $k_{SO_4^{2-}}$ was observed, due to the enhanced H
454 transfer by CHN acting as H-bond acceptor (Dou et al., 2015). With the addition of NaCl, the
455 enhanced H-transfer effect by CHN was inhibited, possibly due to the consumption of ³PS* by
456 Cl⁻. The addition of model CHON species into PS decreased $k_{SO_4^{2-}}$, due to the consumption of
457 ³PS* by CHON species, in agreement with Wang et al. (2023b) who reported increased effective
458 quantum yield of 4-NC when co-photolysis with VL. Further addition of NaCl increased the
459 $k_{SO_4^{2-}}$, possibly due to the consumption of 4-NC by RCS (Wang et al., 2024b), which, to some
460 extent, reduced the loss of ³PS*. Generally, the addition of chloride increased $k_{SO_4^{2-}}$ of PS-
461 CHON but decreased $k_{SO_4^{2-}}$ of PS-CHN. However, the ambient air is characterized by the
462 presence of tens of thousands of chemical compounds. As a result, the interplay among this
463 diverse array of species may occur in ways that exceed current understanding, necessitating
464 additional research to investigate the interactions between different organic compounds more

465 thoroughly.



466

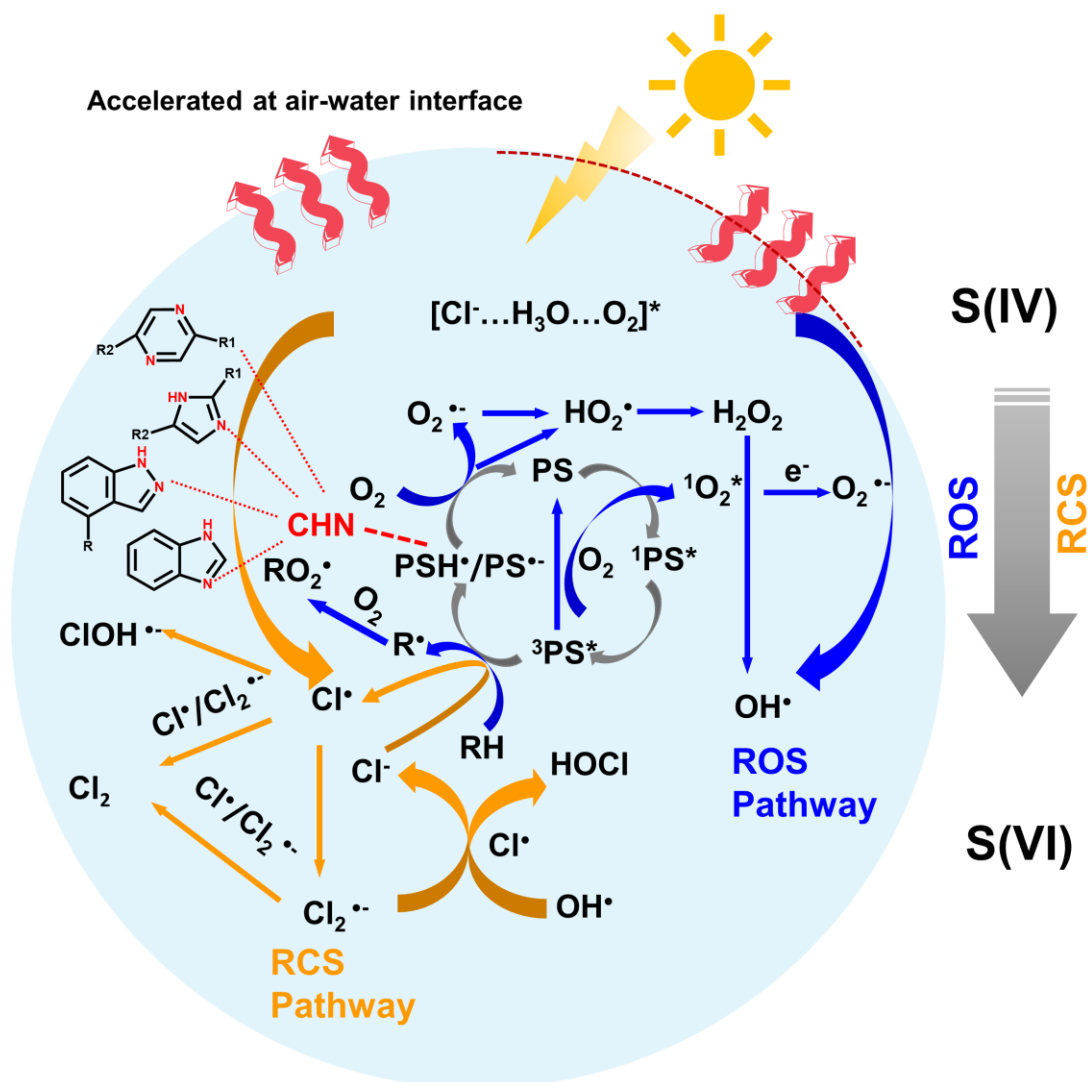
467 Figure 4. (a) Sulfate formation rate and (b) (c) bisulfite decay in RS-NaCl aqueous reactions. 1-0,
468 1-100, and 1-200 refer to the concentration ratios of TOC_{RS} and NaCl, in which 1, 100, 200 represent
469 1 ppm, 100 ppm and 200 ppm, respectively.

470 3.4 Proposed mechanism for sulfate formation

471 A conceptual diagram of PS and chloride mediated ROS and RCS production in the oxidation
472 of S (IV) to S (VI) was shown in Fig. 5. Initially, the PS (e.g., SyrAld and VL) absorb solar
473 radiation and produce the singlet state $^1\text{PS}^*$, which then undergoes a spin conversion through
474 intersystem crossing, leading to the formation of the triplet state $^3\text{PS}^*$. The $^3\text{PS}^*$ can react with
475 molecular oxygen through energy transfer and generate singlet state $^1\text{O}_2^*$, while the $^3\text{PS}^*$ returns
476 to ground state. The $^1\text{O}_2^*$ can then transform to $\text{O}_2^{\cdot-}$ via electron transfer. The $^3\text{PS}^*$ can also react
477 with an H donor (RH, e.g., organic acids, syringol, guaiacol, Table S3), leading to the formation
478 of alkyl or phenoxy radical (R^\bullet) and a ketyl radical (PSH^\bullet). R^\bullet can react with O_2 and form RO_2
479 radicals while PSH^\bullet can transfer an H atom to O_2 and form HO_2^\bullet , returning to its ground state
480 PS. Additionally, $^3\text{PS}^*$ can react with an electron donor, e.g., Cl^- , and form chlorine radicals
481 and PS^\bullet . The formed PS^\bullet then reacts with O_2 and form $\text{O}_2^{\cdot-}$, which undergoes a series of
482 reactions and form HO_2^\bullet , H_2O_2 and OH^\bullet . The above-mentioned reactions are the main processes
483 in the ROS pathway. Recently, Zhang and Chan(2024) have proposed that the reactive chlorine

484 species (RCS) would contribute to sulfate formation. Cao et al. (2024) proposed a mechanism
485 of OH and Cl radicals formation by $[\text{Cl}^- \cdot \text{H}_3\text{O}^+ \cdot \text{O}_2]$ under light irradiation through an electron
486 transfer process. Our results also demonstrate that the addition of Cl^- will affect the oxidation
487 process of S(VI) (Figures 4, S10-S12). Combining the above, the RCS pathway was shown in
488 yellow arrows in Figure 5. The Cl^\bullet can be formed in two pathways, photoexcitation of the $[\text{Cl}^-$
489 $\cdot \text{H}_3\text{O}^+ \cdot \text{O}_2]$ complex that generates Cl radicals in deliquescent BB-NaCl droplets or aqueous
490 BB-NaCl solution (Cao et al., 2024), and PS^* mediated Cl^\bullet formation via electron transfer by
491 Cl^- (Corral Arroyo et al., 2019). The formed Cl^\bullet can then react with each other through radical-
492 radical reactions and produce molecular Cl_2 . The Cl^\bullet can also react with Cl^- or Cl_2^\bullet , forming
493 Cl_2^\bullet or Cl_2 . Cl^\bullet and Cl_2^\bullet can also react with OH and form HOCl. $^3\text{PS}^*$ itself can also oxidize
494 the S(IV) (e.g., dissolved SO_2 or bisulfite) to S(VI). However, significantly lower sulfate
495 formation was found in the presence of N_2 compared to air condition (Figure 2), highlighting
496 the importance of secondary oxidants compared to direct PS^* oxidation. As a consequence,
497 these reactive species, e.g., $\text{OH}^\bullet/\text{HO}_2^\bullet/\text{O}_2^\bullet$ and $\text{Cl}^\bullet/\text{Cl}_2^\bullet$ may all participate in the oxidation of
498 S(IV) to S(VI). In addition, the nitrogen-containing heterocyclic compounds such as pyrazine
499 can act as H-bonding acceptor and facilitate the H transfer, which then generates more ROS
500 (Dou et al., 2015). In light of the absence of substantial fluctuations in chloride concentration
501 (Figure S13 and S14, insignificant chloride concentration change was found even in 10 ppm
502 NaCl addition), it is postulated that chloride ions may function as a reactive medium rather than
503 as direct reactants. In this proposed scenario, the Cl radicals and Cl_2^\bullet intermediates generated
504 during the reaction subsequently undergo reversion back to Cl^- ions, thereby maintaining a
505 relatively constant Cl^- concentration throughout the experimental observations. Note that
506 although ROS and RCS pathways both contribute to the oxidation from S(IV) to S(VI), they
507 may act as competitive relationships due to the co-consumption of PS^* . Therefore, different Cl
508 effects may occur regarding various combinations of reactants (Figure 4, promoting effect in
509 RS_A , inhibiting effects on RS_F).

510



511

512 Figure 5. Conceptual diagram of PS and chloride mediated ROS and RCS production, in the
513 oxidation processes from S(IV) to S(VI)

514 **4 Atmospheric Implication**

515 This study provided laboratory evidence that the PS in biomass burning extracts can enhance
516 the sulfate formation in NaCl particles, primarily by triggering the formation of secondary
517 oxidants under light and air, with less contribution of direct photosensitization via triplets
518 (evidenced by N₂ atmosphere, Figure 2). The sulfate formation rate of BB_F-NaCl particles were
519 ~10 folds higher than that of IS_F-NaCl, following the trends of CS_F-NaCl>RS_F-NaCl>WS_F-
520 NaCl>IS_F-NaCl. Upon UV exposure, the sulfate formation trends shifted to RS_A-NaCl>CS_A-
521 NaCl>WS_A-NaCl>IS_A-NaCl, which might be explained by the effects of chloride (evidenced
522 by aqueous reactions, Figure 4 and Table 1). Interestingly, the incorporation of Cl⁻ into bulk
523 solutions increased the sulfate formation rate in RS_A, while decreased it in RS_F. This seems to
524 be different from our group's previous work where no significant sulfate formation rate was
525 found with the addition of Cl⁻ (Zhang and Chan, 2024). The difference can be explained by the
526 following reasons: 1) differences in PS/Cl⁻, the prior study might use an insufficient PS/Cl⁻ ratio

527 (2:1-1:4) while the current one significantly expands it to 1:200. 2) differences in
528 photosensitizing capacity: the former study used a strong PS, while the current study focused
529 on the real BB (using TOC as metric, with only a small portion of TOC considered as PS). 3)
530 the complexity of the reaction system, the former study focused on mixing two individual
531 species, while in real BB extracts, more complicated reactions may occur. Furthermore, our
532 results using model PS show that although additional model CHN species would increase the
533 sulfate formation by expedited H transfer via acting as H-bond acceptor, the addition of chloride
534 could inhibit the sulfate formation rate, suggesting that the RCS pathway was less efficient in
535 sulfate formation compared to ROS pathway in PS-CHN bulk system (Figure S10 and S11).

536 Previous studies have detected a significant proportion of NOCs, including nitroaromatics
537 (CHON) and reduced nitrogen species (CHN) in biomass burning plumes, wildfires and
538 ambient samples (Zhong et al., 2024; Wang et al., 2017b; Song et al., 2022; Cai et al., 2020).
539 These NOCs are considered as ubiquitous contributors to BrC and can affect global climate and
540 human health. Moreover, recent research has discovered aerosol pollution in marine
541 background regions, with high levels of NOCs when air masses are transported from wildfires
542 or biomass burning events in nearby (Zhong et al., 2024; Qin et al., 2024). These NOCs,
543 combined with reactive gases, may mix with sea-salt aerosols and impact regional air quality
544 in coastal zones. While our prior study has examined the potential interplay between chloride
545 and PS at limited mixing ratios (up to 4:1 in bulk solution) (Zhang and Chan, 2024), this work
546 expanded the Cl/PS ratio to a broader range (200:1) and systematically identified the
547 interactions among different organics, including PS, NOCs, and chloride, using sulfate
548 formation as a compass. This highlights the importance of studying secondary aerosol
549 formation in mixed experimental systems under air pollution complex. Our work suggests that
550 in coastal regions heavily influenced by anthropogenic emissions like biomass burning,
551 especially those near the rice-growing regions or affected by transported wildfire smoke, such
552 as Guangdong, Fujian and Taiwan, the transported BB plumes together with the high RH
553 (Cheung et al., 2015) and abundant reactive gases, would play an inevitable role in sulfate and
554 potentially secondary organic aerosol formation.

555 **Data availability**

556 Datasets are available upon request to the corresponding author, Chak K. Chan
557 (chak.chan@kaust.edu.sa).

558 **Author contributions**

559 RT and CC conceptualized and designed the study. YQ and YC collected the samples. RT
560 performed the experiments, data analysis and wrote the draft. JM provided assistance in data
561 processing. All the authors reviewed, edited and contributed to the scientific discussions.

562 **Competing interests**

563 The authors declare no conflicts of interest.

564 **Acknowledgments**

565 We gratefully acknowledge the support from the Hong Kong Research Grants Council (No.
566 11314222), the National Natural Science Foundation of China (42107115), and the Natural
567 Science Foundation of Shandong Province, China (ZR2021QD111). The authors also thank the
568 University Research Facility in Chemical and Environmental Analysis (UCEA) at The Hong
569 Kong Polytechnic University for the use of its UHPLC-HESI-Orbitrap Mass Spectrometer and
570 Dr Sirius Tse and Dr Chi Hang Chow for assistance with sample analyses.

571 **References**

572 Alexander, B., Allman, D. J., Amos, H. M., Fairlie, T. D., Dachs, J., Hegg, D. A., and Sletten, R. S.:
573 Isotopic constraints on the formation pathways of sulfate aerosol in the marine boundary layer of
574 the subtropical northeast Atlantic Ocean, *Journal of Geophysical Research: Atmospheres*, 117,
575 <https://doi.org/10.1029/2011JD016773>, 2012.

576 Anastasio, C. and Newberg, J. T.: Sources and sinks of hydroxyl radical in sea-salt particles, *Journal*
577 *of Geophysical Research: Atmospheres*, 112, 2007.

578 Andreae, M. O.: Emission of trace gases and aerosols from biomass burning – an updated
579 assessment, *Atmos. Chem. Phys.*, 19, 8523-8546, 10.5194/acp-19-8523-2019, 2019.

580 Bond, T. C., Doherty, S. J., Fahey, D. W., Forster, P. M., Berntsen, T., DeAngelo, B. J., Flanner, M. G.,
581 Ghan, S., Kärcher, B., Koch, D., Kinne, S., Kondo, Y., Quinn, P. K., Sarofim, M. C., Schultz, M. G.,
582 Schulz, M., Venkataraman, C., Zhang, H., Zhang, S., Bellouin, N., Guttikunda, S. K., Hopke, P. K.,
583 Jacobson, M. Z., Kaiser, J. W., Klimont, Z., Lohmann, U., Schwarz, J. P., Shindell, D., Storelvmo, T.,
584 Warren, S. G., and Zender, C. S.: Bounding the role of black carbon in the climate system: A
585 scientific assessment, *Journal of Geophysical Research: Atmospheres*, 118, 5380-5552,
586 <https://doi.org/10.1002/jgrd.50171>, 2013.

587 Cai, J., Zeng, X., Zhi, G., Gligorovski, S., Sheng, G., Yu, Z., Wang, X., and Peng, P.: Molecular
588 composition and photochemical evolution of water-soluble organic carbon (WSOC) extracted
589 from field biomass burning aerosols using high-resolution mass spectrometry, *Atmos. Chem. Phys.*,
590 20, 6115-6128, 10.5194/acp-20-6115-2020, 2020.

591 Calderon-Arrieta, D., Morales, A. C., Hettiyadura, A. P. S., Estock, T. M., Li, C., Rudich, Y., and Laskin,
592 A.: Enhanced Light Absorption and Elevated Viscosity of Atmospheric Brown Carbon through
593 Evaporation of Volatile Components, *Environmental Science & Technology*, 58, 7493-7504,
594 10.1021/acs.est.3c10184, 2024.

595 Cao, Y., Liu, J., Ma, Q., Zhang, C., Zhang, P., Chen, T., Wang, Y., Chu, B., Zhang, X., Francisco, J. S.,
596 and He, H.: Photoactivation of Chlorine and Its Catalytic Role in the Formation of Sulfate Aerosols,
597 *Journal of the American Chemical Society*, 146, 1467-1475, 10.1021/jacs.3c10840, 2024.

598 Chen, J., Li, C., Ristovski, Z., Milic, A., Gu, Y., Islam, M. S., Wang, S., Hao, J., Zhang, H., He, C., Guo,
599 H., Fu, H., Miljevic, B., Morawska, L., Thai, P., Lam, Y. F., Pereira, G., Ding, A., Huang, X., and Dumka,
600 U. C.: A review of biomass burning: Emissions and impacts on air quality, health and climate in
601 China, *Science of The Total Environment*, 579, 1000-1034,
602 <https://doi.org/10.1016/j.scitotenv.2016.11.025>, 2017.

603 Chen, Y., Zheng, P., Wang, Z., Pu, W., Tan, Y., Yu, C., Xia, M., Wang, W., Guo, J., Huang, D., Yan, C.,
604 Nie, W., Ling, Z., Chen, Q., Lee, S., and Wang, T.: Secondary Formation and Impacts of Gaseous
605 Nitro-Phenolic Compounds in the Continental Outflow Observed at a Background Site in South
606 China, *Environmental Science & Technology*, 56, 6933-6943, 10.1021/acs.est.1c04596, 2022a.

607 Chen, Z., Liu, P., Wang, W., Cao, X., Liu, Y.-X., Zhang, Y.-H., and Ge, M.: Rapid Sulfate Formation

608 via Uncatalyzed Autoxidation of Sulfur Dioxide in Aerosol Microdroplets, *Environmental Science &*
609 *Technology*, 56, 7637–7646, 10.1021/acs.est.2c00112, 2022b.

610 Cheng, S.-B., Zhou, C.-H., Yin, H.-M., Sun, J.-L., and Han, K.-L.: OH produced from o-nitrophenol
611 photolysis: A combined experimental and theoretical investigation, *The Journal of chemical physics*,
612 130, 2009.

613 Cheung, H. H., Yeung, M. C., Li, Y. J., Lee, B. P., and Chan, C. K.: Relative humidity-dependent
614 HTDMA measurements of ambient aerosols at the HKUST supersite in Hong Kong, China, *Aerosol*
615 *Science and Technology*, 49, 643–654, 2015.

616 Chi, J. W., Li, W. J., Zhang, D. Z., Zhang, J. C., Lin, Y. T., Shen, X. J., Sun, J. Y., Chen, J. M., Zhang, X.
617 Y., Zhang, Y. M., and Wang, W. X.: Sea salt aerosols as a reactive surface for inorganic and organic
618 acidic gases in the Arctic troposphere, *Atmos. Chem. Phys.*, 15, 11341–11353, 10.5194/acp-15-
619 11341-2015, 2015.

620 Corral Arroyo, P., Aellig, R., Alpert, P. A., Volkamer, R., and Ammann, M.: Halogen activation and
621 radical cycling initiated by imidazole-2-carboxaldehyde photochemistry, *Atmospheric Chemistry*
622 *and Physics*, 19, 10817–10828, 2019.

623 Dou, J., Lin, P., Kuang, B.-Y., and Yu, J. Z.: Reactive Oxygen Species Production Mediated by Humic-
624 like Substances in Atmospheric Aerosols: Enhancement Effects by Pyridine, Imidazole, and Their
625 Derivatives, *Environmental Science & Technology*, 49, 6457–6465, 10.1021/es5059378, 2015.

626 Fang, Z., Deng, W., Zhang, Y., Ding, X., Tang, M., Liu, T., Hu, Q., Zhu, M., Wang, Z., Yang, W., Huang,
627 Z., Song, W., Bi, X., Chen, J., Sun, Y., George, C., and Wang, X.: Open burning of rice, corn and
628 wheat straws: primary emissions, photochemical aging, and secondary organic aerosol formation,
629 *Atmos. Chem. Phys.*, 17, 14821–14839, 10.5194/acp-17-14821-2017, 2017.

630 Felber, T., Schaefer, T., and Herrmann, H.: Five-Membered Heterocycles as Potential
631 Photosensitizers in the Tropospheric Aqueous Phase: Photophysical Properties of Imidazole-2-
632 carboxaldehyde, 2-Furaldehyde, and 2-Acetylfuran, *The Journal of Physical Chemistry A*, 124,
633 10029–10039, 10.1021/acs.jpca.0c07028, 2020.

634 Felber, T., Schaefer, T., He, L., and Herrmann, H.: Aromatic Carbonyl and Nitro Compounds as
635 Photosensitizers and Their Photophysical Properties in the Tropospheric Aqueous Phase, *The*
636 *Journal of Physical Chemistry A*, 125, 5078–5095, 10.1021/acs.jpca.1c03503, 2021.

637 Fu, H., Ciuraru, R., Dupart, Y., Passananti, M., Tinel, L., Rossignol, S., Perrier, S., Donaldson, D. J.,
638 Chen, J., and George, C.: Photosensitized Production of Atmospherically Reactive Organic
639 Compounds at the Air/Aqueous Interface, *Journal of the American Chemical Society*, 137, 8348–
640 8351, 10.1021/jacs.5b04051, 2015.

641 Fushimi, A., Saitoh, K., Hayashi, K., Ono, K., Fujitani, Y., Villalobos, A. M., Shelton, B. R., Takami, A.,
642 Tanabe, K., and Schauer, J. J.: Chemical characterization and oxidative potential of particles emitted
643 from open burning of cereal straws and rice husk under flaming and smoldering conditions,
644 *Atmospheric Environment*, 163, 118–127, <https://doi.org/10.1016/j.atmosenv.2017.05.037>, 2017.

645 Gantt, B. and Meskhidze, N.: The physical and chemical characteristics of marine primary organic
646 aerosol: a review, *Atmos. Chem. Phys.*, 13, 3979–3996, 10.5194/acp-13-3979-2013, 2013.

647 Gen, M., Zhang, R., Huang, D. D., Li, Y., and Chan, C. K.: Heterogeneous SO₂ Oxidation in Sulfate
648 Formation by Photolysis of Particulate Nitrate, *Environmental Science & Technology Letters*, 6, 86–
649 91, 10.1021/acs.estlett.8b00681, 2019a.

650 Gen, M., Zhang, R., Huang, D. D., Li, Y., and Chan, C. K.: Heterogeneous Oxidation of SO₂ in Sulfate
651 Production during Nitrate Photolysis at 300 nm: Effect of pH, Relative Humidity, Irradiation

652 Intensity, and the Presence of Organic Compounds, *Environmental Science & Technology*, 53,
653 8757-8766, 10.1021/acs.est.9b01623, 2019b.

654 Gómez Alvarez, E., Wortham, H., Strekowski, R., Zetzsch, C., and Gligorovski, S.: Atmospheric
655 Photosensitized Heterogeneous and Multiphase Reactions: From Outdoors to Indoors,
656 *Environmental Science & Technology*, 46, 1955-1963, 10.1021/es2019675, 2012.

657 Guo, S. and Li, H.: Photolysis of nitrophenols in gas phase and aqueous environment: a potential
658 daytime source for atmospheric nitrous acid (HONO), *Environmental Science: Atmospheres*, 3,
659 143-155, 2023.

660 Hu, W., Zhou, H., Chen, W., Ye, Y., Pan, T., Wang, Y., Song, W., Zhang, H., Deng, W., Zhu, M., Wang,
661 C., Wu, C., Ye, C., Wang, Z., Yuan, B., Huang, S., Shao, M., Peng, Z., Day, D. A., Campuzano-Jost, P.,
662 Lambe, A. T., Worsnop, D. R., Jimenez, J. L., and Wang, X.: Oxidation Flow Reactor Results in a
663 Chinese Megacity Emphasize the Important Contribution of S/IVOCs to Ambient SOA Formation,
664 *Environmental Science & Technology*, 56, 6880-6893, 10.1021/acs.est.1c03155, 2022.

665 Huang, G., Wang, S., Chang, X., Cai, S., Zhu, L., Li, Q., and Jiang, J.: Emission factors and chemical
666 profile of I/SVOCs emitted from household biomass stove in China, *Science of The Total*
667 *Environment*, 842, 156940, <https://doi.org/10.1016/j.scitotenv.2022.156940>, 2022a.

668 Huang, R.-J., Yang, L., Shen, J., Yuan, W., Gong, Y., Ni, H., Duan, J., Yan, J., Huang, H., You, Q., and
669 Li, Y. J.: Chromophoric Fingerprinting of Brown Carbon from Residential Biomass Burning,
670 *Environmental Science & Technology Letters*, 9, 102-111, 10.1021/acs.estlett.1c00837, 2022b.

671 Huang, S., Wu, Z., Poulain, L., van Pinxteren, M., Merkel, M., Assmann, D., Herrmann, H., and
672 Wiedensohler, A.: Source apportionment of the organic aerosol over the Atlantic Ocean from
673 53° N to 53° S: significant contributions from marine emissions and long-range
674 transport, *Atmos. Chem. Phys.*, 18, 18043-18062, 10.5194/acp-18-18043-2018, 2018.

675 Jammoul, A., Dumas, S., D'Anna, B., and George, C.: Photoinduced oxidation of sea salt halides by
676 aromatic ketones: a source of halogenated radicals, *Atmos. Chem. Phys.*, 9, 4229-4237,
677 10.5194/acp-9-4229-2009, 2009.

678 Jiang, H., Carena, L., He, Y., Wang, Y., Zhou, W., Yang, L., Luan, T., Li, X., Brigante, M., Vione, D., and
679 Gligorovski, S.: Photosensitized Degradation of DMSO Initiated by PAHs at the Air-Water Interface,
680 as an Alternative Source of Organic Sulfur Compounds to the Atmosphere, *Journal of Geophysical*
681 *Research: Atmospheres*, 126, e2021JD035346, <https://doi.org/10.1029/2021JD035346>, 2021.

682 Jones, M. W., Abatzoglou, J. T., Veraverbeke, S., Andela, N., Lasslop, G., Forkel, M., Smith, A. J. P.,
683 Burton, C., Betts, R. A., van der Werf, G. R., Sitch, S., Canadell, J. G., Santín, C., Kolden, C., Doerr, S.
684 H., and Le Quééré, C.: Global and Regional Trends and Drivers of Fire Under Climate Change,
685 *Reviews of Geophysics*, 60, e2020RG000726, <https://doi.org/10.1029/2020RG000726>, 2022.

686 Kalogridis, A. C., Popovicheva, O. B., Engling, G., Diapouli, E., Kawamura, K., Tachibana, E., Ono, K.,
687 Kozlov, V. S., and Eleftheriadis, K.: Smoke aerosol chemistry and aging of Siberian biomass burning
688 emissions in a large aerosol chamber, *Atmospheric Environment*, 185, 15-28,
689 <https://doi.org/10.1016/j.atmosenv.2018.04.033>, 2018.

690 Kim, Y. H., Warren, S. H., Krantz, Q. T., King, C., Jaskot, R., Preston, W. T., George, B. J., Hays, M. D.,
691 Landis, M. S., and Higuchi, M.: Mutagenicity and lung toxicity of smoldering vs. flaming emissions
692 from various biomass fuels: implications for health effects from wildland fires, *Environmental health*
693 *perspectives*, 126, 017011, 2018.

694 Kim, Y. H., Warren, S. H., Kooter, I., Williams, W. C., George, I. J., Vance, S. A., Hays, M. D., Higuchi,
695 M. A., Gavett, S. H., DeMarini, D. M., Jaspers, I., and Gilmour, M. I.: Chemistry, lung toxicity and

696 mutagenicity of burn pit smoke-related particulate matter, *Particle and Fibre Toxicology*, 18, 45,
697 10.1186/s12989-021-00435-w, 2021.

698 Kipp, B. H., Faraj, C., Li, G., and Njus, D.: Imidazole facilitates electron transfer from organic
699 reductants, *Bioelectrochemistry*, 64, 7-13, <https://doi.org/10.1016/j.bioelechem.2003.12.010>, 2004.

700 Koch, B. P. and Dittmar, T.: From mass to structure: An aromaticity index for high-resolution mass
701 data of natural organic matter, *Rapid communications in mass spectrometry*, 20, 926-932, 2006.

702 Laskin, A., Laskin, J., and Nizkorodov, S. A.: Chemistry of Atmospheric Brown Carbon, *Chemical*
703 *Reviews*, 115, 4335-4382, 10.1021/cr5006167, 2015.

704 Laskin, A., Smith, J. S., and Laskin, J.: Molecular Characterization of Nitrogen-Containing Organic
705 Compounds in Biomass Burning Aerosols Using High-Resolution Mass Spectrometry,
706 *Environmental Science & Technology*, 43, 3764-3771, 10.1021/es803456n, 2009.

707 Li, F., Zhou, S., Zhao, J., Hang, J., Lu, H., Li, X., Gao, M., Li, Y., and Wang, X.: Aqueous
708 Photosensitization of Syringaldehyde: Reactivity, Effects of Environmental Factors, and Formation
709 of Brown Carbon Products, *ACS Earth and Space Chemistry*, 2024.

710 Li, S., Jiang, X., Roveretto, M., George, C., Liu, L., Jiang, W., Zhang, Q., Wang, W., Ge, M., and Du,
711 L.: Photochemical aging of atmospherically reactive organic compounds involving brown carbon
712 at the air-aqueous interface, *Atmos. Chem. Phys.*, 19, 9887-9902, 10.5194/acp-19-9887-2019,
713 2019.

714 Liang, Z., Li, Y., Go, B. R., and Chan, C. K.: Complexities of Photosensitization in Atmospheric
715 Particles, *ACS ES&T Air*, 10.1021/acsestair.4c00112, 2024.

716 Lin, P., Rincon, A. G., Kalberer, M., and Yu, J. Z.: Elemental Composition of HULIS in the Pearl River
717 Delta Region, China: Results Inferred from Positive and Negative Electrospray High Resolution
718 Mass Spectrometric Data, *Environmental Science & Technology*, 46, 7454-7462,
719 10.1021/es300285d, 2012.

720 Lin, P., Fleming, L. T., Nizkorodov, S. A., Laskin, J., and Laskin, A.: Comprehensive Molecular
721 Characterization of Atmospheric Brown Carbon by High Resolution Mass Spectrometry with
722 Electrospray and Atmospheric Pressure Photoionization, *Analytical Chemistry*, 90, 12493-12502,
723 10.1021/acs.analchem.8b02177, 2018.

724 Liu, D., Zhang, Y., Zhong, S., Chen, S., Xie, Q., Zhang, D., Zhang, Q., Hu, W., Deng, J., Wu, L., Ma,
725 C., Tong, H., and Fu, P.: Large differences of highly oxygenated organic molecules (HOMs) and
726 low-volatile species in secondary organic aerosols (SOAs) formed from ozonolysis of β -pinene
727 and limonene, *Atmos. Chem. Phys.*, 23, 8383-8402, 10.5194/acp-23-8383-2023, 2023a.

728 Liu, H., Pei, X., Zhang, F., Song, Y., Kuang, B., Xu, Z., and Wang, Z.: Relative Humidity Dependence
729 of Growth Factor and Real Refractive Index for Sea Salt/Malonic Acid Internally Mixed Aerosols,
730 *Journal of Geophysical Research: Atmospheres*, 128, e2022JD037579,
731 <https://doi.org/10.1029/2022JD037579>, 2023b.

732 Liu, Y., Wang, T., Fang, X., Deng, Y., Cheng, H., Nabi, I., and Zhang, L.: Brown carbon: An underlying
733 driving force for rapid atmospheric sulfate formation and haze event, *Science of the Total*
734 *Environment*, 734, 139415, 2020.

735 Mabato, B. R. G., Li, Y. J., Huang, D. D., Wang, Y., and Chan, C. K.: Comparison of aqueous secondary
736 organic aerosol (aqSOA) product distributions from guaiacol oxidation by non-phenolic and
737 phenolic methoxybenzaldehydes as photosensitizers in the absence and presence of ammonium
738 nitrate, *Atmos. Chem. Phys.*, 23, 2859-2875, 10.5194/acp-23-2859-2023, 2023.

739 Mabato, B. R. G., Lyu, Y., Ji, Y., Li, Y. J., Huang, D. D., Li, X., Nah, T., Lam, C. H., and Chan, C. K.:

740 Aqueous secondary organic aerosol formation from the direct photosensitized oxidation of vanillin
741 in the absence and presence of ammonium nitrate, *Atmos. Chem. Phys.*, 22, 273-293,
742 10.5194/acp-22-273-2022, 2022.

743 Mao, J., Ren, X., Brune, W. H., Olson, J. R., Crawford, J. H., Fried, A., Huey, L. G., Cohen, R. C., Heikes,
744 B., Singh, H. B., Blake, D. R., Sachse, G. W., Diskin, G. S., Hall, S. R., and Shetter, R. E.: Airborne
745 measurement of OH reactivity during INTEX-B, *Atmos. Chem. Phys.*, 9, 163-173, 10.5194/acp-9-
746 163-2009, 2009.

747 Martins-Costa, M. T., Anglada, J. M., Francisco, J. S., and Ruiz-López, M. F.: Photosensitization
748 mechanisms at the air-water interface of aqueous aerosols, *Chemical science*, 13, 2624-2631, 2022.

749 Mohr, C., Lopez-Hilfiker, F. D., Zotter, P., Prévôt, A. S. H., Xu, L., Ng, N. L., Herndon, S. C., Williams,
750 L. R., Franklin, J. P., Zahniser, M. S., Worsnop, D. R., Knighton, W. B., Aiken, A. C., Gorkowski, K. J.,
751 Dubey, M. K., Allan, J. D., and Thornton, J. A.: Contribution of Nitrated Phenols to Wood Burning
752 Brown Carbon Light Absorption in Detling, United Kingdom during Winter Time, *Environmental
753 Science & Technology*, 47, 6316-6324, 10.1021/es400683v, 2013.

754 Parker, K. M. and Mitch, W. A.: Halogen radicals contribute to photooxidation in coastal and
755 estuarine waters, *Proceedings of the National Academy of Sciences*, 113, 5868-5873, 2016.

756 Peng, Z. and Jimenez, J. L.: Radical chemistry in oxidation flow reactors for atmospheric chemistry
757 research, *Chemical Society Reviews*, 49, 2570-2616, 2020.

758 Pozzoli, L., Gilardoni, S., Perrone, M. G., de Gennaro, G., de Rienzo, M., and Vione, D.: POLYCYCLIC
759 AROMATIC HYDROCARBONS IN THE ATMOSPHERE: MONITORING, SOURCES, SINKS AND FATE.
760 I: MONITORING AND SOURCES, *Annali di Chimica*, 94, 17-33,
761 <https://doi.org/10.1002/adic.200490002>, 2004.

762 Qin, Y., Wang, H., Wang, Y., Lu, X., Tang, H., Zhang, J., Li, L., and Fan, S.: Wildfires in Southeast Asia
763 pollute the atmosphere in the northern South China Sea, *Science Bulletin*, 69, 1011-1015,
764 <https://doi.org/10.1016/j.scib.2024.02.026>, 2024.

765 Qiu, Y., Wu, X., Zhang, Y., Xu, L., Hong, Y., Chen, J., Chen, X., and Deng, J.: Aerosol light absorption
766 in a coastal city in Southeast China: Temporal variations and implications for brown carbon, *Journal
767 of Environmental Sciences*, 80, 257-266, <https://doi.org/10.1016/j.jes.2019.01.002>, 2019.

768 Rowe, J. P., Lambe, A. T., and Brune, W. H.: Technical Note: Effect of varying the $\lambda = 185$ and
769 254 nm photon flux ratio on radical generation in oxidation flow reactors, *Atmos. Chem.
770 Phys.*, 20, 13417-13424, 10.5194/acp-20-13417-2020, 2020.

771 Safiarian, M. S., Ugboya, A., Khan, I., Marichev, K. O., and Grant, K. B.: New Insights into the
772 Phototoxicity of Anthracene-Based Chromophores: The Chloride Salt Effect, *Chemical Research in
773 Toxicology*, 36, 1002-1020, 10.1021/acs.chemrestox.2c00235, 2023.

774 Salvador, C. M. G., Tang, R., Priestley, M., Li, L. J., Tsiligiannis, E., Le Breton, M., Zhu, W., Zeng, L.,
775 Wang, H., and Yu, Y.: Ambient nitro-aromatic compounds-biomass burning versus secondary
776 formation in rural China, *Atmospheric Chemistry and Physics Discussions*, 2020, 1-36, 2020.

777 Sangwan, M. and Zhu, L.: Absorption cross sections of 2-nitrophenol in the 295-400 nm region
778 and photolysis of 2-nitrophenol at 308 and 351 nm, *The Journal of Physical Chemistry A*, 120,
779 9958-9967, 2016.

780 Sangwan, M. and Zhu, L.: Role of Methyl-2-nitrophenol Photolysis as a Potential Source of OH
781 Radicals in the Polluted Atmosphere: Implications from Laboratory Investigation, *The Journal of
782 Physical Chemistry A*, 122, 1861-1872, 10.1021/acs.jpca.7b11235, 2018.

783 Song, J., Li, M., Zou, C., Cao, T., Fan, X., Jiang, B., Yu, Z., Jia, W., and Peng, P. a.: Molecular

784 Characterization of Nitrogen-Containing Compounds in Humic-like Substances Emitted from
785 Biomass Burning and Coal Combustion, *Environmental Science & Technology*, 56, 119-130,
786 10.1021/acs.est.1c04451, 2022.

787 Song, K., Tang, R., Li, A., Wan, Z., Zhang, Y., Gong, Y., Lv, D., Lu, S., Tan, Y., Yan, S., Yan, S., Zhang,
788 J., Fan, B., Chan, C. K., and Guo, S.: Particulate organic emissions from incense-burning smoke:
789 Chemical compositions and emission characteristics, *Science of The Total Environment*, 897,
790 165319, <https://doi.org/10.1016/j.scitotenv.2023.165319>, 2023.

791 Tang, R., Zhang, R., Ma, J., Song, K., Mabato, B. R. G., Cuevas, R. A. I., Zhou, L., Liang, Z., Vogel, A.
792 L., Guo, S., and Chan, C. K.: Sulfate Formation by Photosensitization in Mixed Incense Burning–
793 Sodium Chloride Particles: Effects of RH, Light Intensity, and Aerosol Aging, *Environmental Science
794 & Technology*, 57, 10295-10307, 10.1021/acs.est.3c02225, 2023.

795 Teich, M., van Pinxteren, D., Kecorius, S., Wang, Z., and Herrmann, H.: First quantification of
796 imidazoles in ambient aerosol particles: potential photosensitizers, brown carbon constituents, and
797 hazardous components, *Environmental science & technology*, 50, 1166-1173, 2016.

798 Ting, Y., Mitchell, E. J. S., Allan, J. D., Liu, D., Spracklen, D. V., Williams, A., Jones, J. M., Lea-Langton,
799 A. R., McFiggans, G., and Coe, H.: Mixing State of Carbonaceous Aerosols of Primary Emissions
800 from “Improved” African Cookstoves, *Environmental Science & Technology*, 52, 10134-10143,
801 10.1021/acs.est.8b00456, 2018.

802 Tkacik, D. S., Lambe, A. T., Jathar, S., Li, X., Presto, A. A., Zhao, Y., Blake, D., Meinardi, S., Jayne, J. T.,
803 Croteau, P. L., and Robinson, A. L.: Secondary Organic Aerosol Formation from in-Use Motor
804 Vehicle Emissions Using a Potential Aerosol Mass Reactor, *Environmental Science & Technology*,
805 48, 11235-11242, 10.1021/es502239v, 2014.

806 van Pinxteren, M., Fiedler, B., van Pinxteren, D., Iinuma, Y., Körtzinger, A., and Herrmann, H.:
807 Chemical characterization of sub-micrometer aerosol particles in the tropical Atlantic Ocean:
808 marine and biomass burning influences, *Journal of Atmospheric Chemistry*, 72, 105-125,
809 10.1007/s10874-015-9307-3, 2015.

810 Wang, K., Zhang, Y., Tong, H., Han, J., Fu, P., Huang, R.-J., Zhang, H., and Hoffmann, T.: Molecular-
811 Level Insights into the Relationship between Volatility of Organic Aerosol Constituents and PM_{2.5}
812 Air Pollution Levels: A Study with Ultrahigh-Resolution Mass Spectrometry, *Environmental Science
813 & Technology*, 58, 7947-7957, 10.1021/acs.est.3c10662, 2024a.

814 Wang, N., Zhou, D., Liu, H., Tu, Y., Ma, Y., and Li, Y.: Triplet-Excited Dissolved Organic Matter
815 Efficiently Promoted Atmospheric Sulfate Production: Kinetics and Mechanisms, *Separations*, 10,
816 335, 2023a.

817 Wang, S., Liu, T., Jang, J., Abbatt, J. P. D., and Chan, A. W. H.: Heterogeneous interactions between
818 SO₂ and organic peroxides in submicron aerosol, *Atmos. Chem. Phys.*, 21, 6647-6661,
819 10.5194/acp-21-6647-2021, 2021a.

820 Wang, T., Deng, L., Tan, C., Hu, J., and Singh, R. P.: Comparative analysis of chlorinated disinfection
821 byproducts formation from 4-nitrophenol and 2-amino-4-nitrophenol during UV/post-
822 chlorination, *Science of The Total Environment*, 927, 172200,
823 <https://doi.org/10.1016/j.scitotenv.2024.172200>, 2024b.

824 Wang, W., Liu, Y., Wang, T., Ge, Q., Li, K., Liu, J., You, W., Wang, L., Xie, L., Fu, H., Chen, J., and
825 Zhang, L.: Significantly Accelerated Photosensitized Formation of Atmospheric Sulfate at the Air–
826 Water Interface of Microdroplets, *Journal of the American Chemical Society*, 146, 6580-6590,
827 10.1021/jacs.3c11892, 2024c.

828 Wang, X., Gemayel, R., Baboornian, V. J., Li, K., Boreave, A., Dubois, C., Tomaz, S., Perrier, S.,
829 Nizkorodov, S. A., and George, C.: Naphthalene-derived secondary organic aerosols interfacial
830 photosensitizing properties, *Geophysical Research Letters*, 48, e2021GL093465, 2021b.

831 Wang, X., Gu, R., Wang, L., Xu, W., Zhang, Y., Chen, B., Li, W., Xue, L., Chen, J., and Wang, W.:
832 Emissions of fine particulate nitrated phenols from the burning of five common types of biomass,
833 *Environmental Pollution*, 230, 405-412, <https://doi.org/10.1016/j.envpol.2017.06.072>, 2017a.

834 Wang, X., Gemayel, R., Hayeck, N., Perrier, S., Charbonnel, N., Xu, C., Chen, H., Zhu, C., Zhang, L.,
835 Wang, L., Nizkorodov, S. A., Wang, X., Wang, Z., Wang, T., Mellouki, A., Riva, M., Chen, J., and
836 George, C.: Atmospheric Photosensitization: A New Pathway for Sulfate Formation, *Environmental
837 Science & Technology*, 54, 3114-3120, 10.1021/acs.est.9b06347, 2020a.

838 Wang, Y., Hu, M., Xu, N., Qin, Y., Wu, Z., Zeng, L., Huang, X., and He, L.: Chemical composition and
839 light absorption of carbonaceous aerosols emitted from crop residue burning: influence of
840 combustion efficiency, *Atmos. Chem. Phys.*, 20, 13721-13734, 10.5194/acp-20-13721-2020,
841 2020b.

842 Wang, Y., Qiu, T., Zhang, C., Hao, T., Mabato, B. R. G., Zhang, R., Gen, M., Chan, M. N., Huang, D.
843 D., and Ge, X.: Co-photolysis of mixed chromophores affects atmospheric lifetimes of brown
844 carbon, *Environmental Science: Atmospheres*, 3, 1145-1158, 2023b.

845 Wang, Y., Hu, M., Lin, P., Guo, Q., Wu, Z., Li, M., Zeng, L., Song, Y., Zeng, L., Wu, Y., Guo, S., Huang,
846 X., and He, L.: Molecular Characterization of Nitrogen-Containing Organic Compounds in Humic-
847 like Substances Emitted from Straw Residue Burning, *Environmental Science & Technology*, 51,
848 5951-5961, 10.1021/acs.est.7b00248, 2017b.

849 Wei, Z., Li, Y., Cooks, R. G., and Yan, X.: Accelerated reaction kinetics in microdroplets: Overview
850 and recent developments, *Annual Review of Physical Chemistry*, 71, 31-51, 2020.

851 Wu, C.-H., Yuan, C.-S., Yen, P.-H., Yeh, M.-J., and Soong, K.-Y.: Diurnal and seasonal variation,
852 chemical characteristics, and source identification of marine fine particles at two remote islands in
853 South China Sea: A superimposition effect of local emissions and long-range transport,
854 *Atmospheric Environment*, 270, 118889, <https://doi.org/10.1016/j.atmosenv.2021.118889>, 2022.

855 Xie, M., Chen, X., Hays, M. D., and Holder, A. L.: Composition and light absorption of N-containing
856 aromatic compounds in organic aerosols from laboratory biomass burning, *Atmos. Chem. Phys.*,
857 19, 2899-2915, 10.5194/acp-19-2899-2019, 2019.

858 Yang, M., Zhang, H., Chang, F., and Hu, X.: Self-sensitized photochlorination of benzo[a]pyrene in
859 saline water under simulated solar light irradiation, *Journal of Hazardous Materials*, 408, 124445,
860 <https://doi.org/10.1016/j.jhazmat.2020.124445>, 2021.

861 Yao, M., Zhao, Y., Hu, M., Huang, D., Wang, Y., Yu, J. Z., and Yan, N.: Multiphase reactions between
862 secondary organic aerosol and sulfur dioxide: kinetics and contributions to sulfate formation and
863 aerosol aging, *Environmental Science & Technology Letters*, 6, 768-774, 2019.

864 Ye, C., Lu, K., Song, H., Mu, Y., Chen, J., and Zhang, Y.: A critical review of sulfate aerosol formation
865 mechanisms during winter polluted periods, *Journal of Environmental Sciences*, 123, 387-399,
866 <https://doi.org/10.1016/j.jes.2022.07.011>, 2023.

867 Ye, J., Abbatt, J. P., and Chan, A. W.: Novel pathway of SO₂ oxidation in the atmosphere: reactions
868 with monoterpene ozonolysis intermediates and secondary organic aerosol, *Atmospheric
869 Chemistry and Physics*, 18, 5549-5565, 2018.

870 You, B., Li, S., Tsona, N. T., Li, J., Xu, L., Yang, Z., Cheng, S., Chen, Q., George, C., Ge, M., and Du, L.:
871 Environmental Processing of Short-Chain Fatty Alcohols Induced by Photosensitized Chemistry of

872 Brown Carbons, ACS Earth and Space Chemistry, 4, 631-640,
873 10.1021/acsearthspacechem.0c00023, 2020.

874 Zhang, L., Hu, B., Liu, X., Luo, Z., Xing, R., Li, Y., Xiong, R., Li, G., Cheng, H., Lu, Q., Shen, G., and Tao,
875 S.: Variabilities in Primary N-Containing Aromatic Compound Emissions from Residential Solid Fuel
876 Combustion and Implications for Source Tracers, Environmental Science & Technology, 56, 13622-
877 13633, 10.1021/acs.est.2c03000, 2022.

878 Zhang, R. and Chan, C. K.: Simultaneous formation of sulfate and nitrate via co-uptake of SO₂
879 and NO₂ by aqueous NaCl droplets: combined effect of nitrate photolysis and chlorine chemistry,
880 Atmospheric Chemistry and Physics, 23, 6113-6126, 2023a.

881 Zhang, R. and Chan, C. K.: Simultaneous formation of sulfate and nitrate via co-uptake of SO₂ and
882 NO₂ by aqueous NaCl droplets: combined effect of nitrate photolysis and chlorine chemistry,
883 Atmos. Chem. Phys., 23, 6113-6126, 10.5194/acp-23-6113-2023, 2023b.

884 Zhang, R. and Chan, C. K.: Enhanced Sulfate Formation through Synergistic Effects of Chlorine
885 Chemistry and Photosensitization in Atmospheric Particles, ACS ES&T Air, 1, 92-102,
886 10.1021/acsestair.3c00030, 2024.

887 Zhang, R., Gen, M., Huang, D., Li, Y., and Chan, C. K.: Enhanced Sulfate Production by Nitrate
888 Photolysis in the Presence of Halide Ions in Atmospheric Particles, Environmental Science &
889 Technology, 54, 3831-3839, 10.1021/acs.est.9b06445, 2020a.

890 Zhang, S., Li, D., Ge, S., Wu, C., Xu, X., Liu, X., Li, R., Zhang, F., and Wang, G.: Elucidating the
891 Mechanism on the Transition-Metal Ion-Synergetic-Catalyzed Oxidation of SO₂ with Implications
892 for Sulfate Formation in Beijing Haze, Environmental Science & Technology, 58, 2912-2921,
893 10.1021/acs.est.3c08411, 2024.

894 Zhang, S., Li, D., Ge, S., Liu, S., Wu, C., Wang, Y., Chen, Y., Lv, S., Wang, F., Meng, J., and Wang, G.:
895 Rapid sulfate formation from synergetic oxidation of SO₂ by O₃ and NO₂ under ammonia-rich
896 conditions: Implications for the explosive growth of atmospheric PM_{2.5} during haze events in
897 China, Science of The Total Environment, 772, 144897,
898 <https://doi.org/10.1016/j.scitotenv.2020.144897>, 2021a.

899 Zhang, T., Dong, J., Zhang, C., Kong, D., Ji, Y., Zhou, Q., and Lu, J.: Photo-transformation of
900 acetaminophen sensitized by fluoroquinolones in the presence of bromide, Chemosphere, 327,
901 138525, <https://doi.org/10.1016/j.chemosphere.2023.138525>, 2023.

902 Zhang, Y., Wang, K., Tong, H., Huang, R.-J., and Hoffmann, T.: The maximum carbonyl ratio (MCR)
903 as a new index for the structural classification of secondary organic aerosol components, Rapid
904 Communications in Mass Spectrometry, 35, e9113, <https://doi.org/10.1002/rcm.9113>, 2021b.

905 Zhang, Y., Bao, F., Li, M., Xia, H., Huang, D., Chen, C., and Zhao, J.: Photoinduced Uptake and
906 Oxidation of SO₂ on Beijing Urban PM_{2.5}, Environmental Science & Technology, 54, 14868-14876,
907 10.1021/acs.est.0c01532, 2020b.

908 Zhao, R., Zhang, Q., Xu, X., Wang, W., Zhao, W., Zhang, W., and Zhang, Y.: Effect of photooxidation
909 on size distribution, light absorption, and molecular compositions of smoke particles from rice
910 straw combustion, Environmental Pollution, 311, 119950,
911 <https://doi.org/10.1016/j.envpol.2022.119950>, 2022.

912 Zherebker, A., Rukhovich, G. D., Sarycheva, A., Lechtenfeld, O. J., and Nikolaev, E. N.: Aromaticity
913 Index with Improved Estimation of Carboxyl Group Contribution for Biogeochemical Studies,
914 Environmental Science & Technology, 56, 2729-2737, 10.1021/acs.est.1c04575, 2022.

915 Zhong, S., Liu, R., Yue, S., Wang, P., Zhang, Q., Ma, C., Deng, J., Qi, Y., Zhu, J., and Liu, C.-Q.:

916 Peatland Wildfires Enhance Nitrogen-Containing Organic Compounds in Marine Aerosols over
917 the Western Pacific, *Environmental Science & Technology*, 2024.
918 Zhou, L., Liang, Z., Mabato, B. R. G., Cuevas, R. A. I., Tang, R., Li, M., Cheng, C., and Chan, C. K.:
919 Sulfate formation via aerosol-phase SO₂ oxidation by model biomass burning photosensitizers:
920 3,4-dimethoxybenzaldehyde, vanillin and syringaldehyde using single-particle mixing-state
921 analysis, *Atmos. Chem. Phys.*, 23, 5251-5261, 10.5194/acp-23-5251-2023, 2023.
922